Meteoritics & Planetary Science 40, Nr 7, 1073–1101 (2005)
Abstract available online at http://meteoritics.org

Petrography and geochemistry of the LaPaz Icefield basaltic lunar meteorite and source crater pairing with Northwest Africa 032

Ryan A. ZEIGLER*, Randy L. KOROTEV, Bradley L. JOLLIFF, and Larry A. HASKIN

Washington University, Department of Earth and Planetary Science, One Brookings Drive, Saint Louis, Missouri 63130, USA
*Corresponding author. E-mail: zeigler@levee.wustl.edu

(Received 30 May 2005; revision accepted 22 June 2005)

Abstract–We report on the bulk composition and petrography of four new basaltic meteorites found in Antarctica—LAP (LaPaz Icefield) 02205, LAP 02224, LAP 02226, and LAP 02436—and compare the LAP meteorites to other lunar mare basalts. The LAP meteorites are coarse-grained (up to 1.5 mm), subophitic low-Ti basalts composed predominantly of pyroxene and plagioclase, with minor amounts of olivine, ilmenite, and a groundmass dominated by fayalite and cristobalite. All of our observations and results support the hypothesis that the LAP stones are mutually paired with each other. In detail, the geochemistry of LAP is unlike those of any previously studied lunar basalt except lunar meteorite NWA (Northwest Africa) 032. The similarities between LAP and NWA 032 are so strong that the two meteorites are almost certainly source crater paired and could be two different samples of a single basalt flow. Petrogenetic modeling suggests that the parent melt of LAP (and NWA 032) is generally similar to Apollo 15 low-Ti, yellow picritic glass beads, and that the source region for LAP comes from a similar region of the lunar mantle as previously analyzed lunar basalts.

INTRODUCTION

To date, approximately 32 lunar meteorites have been discovered. Although the locations of source craters or regions of the Moon from which any one of them originates is speculative (e.g., Ryder and Ostertag 1983; Fagan et al. 2002; Gnos et al. 2004), there is strong evidence that certain lunar meteorites derive from the same crater as lunar meteorites that fell elsewhere on Earth, that is, that some lunar meteorites are launch paired or source crater paired with others (Warren 1994; Arai and Warren 1999; Korotev et al. 2003a, b). During the 2002 Antarctic Search for Meteorites (ANSMET), the field team collected four basaltic meteorites on the LaPaz ice field (LAP): LAP 02205 (1.23 kg), LAP 02224 (0.25 kg), LAP 02226 (0.24 kg), and LAP 02436 (0.06 kg). During the following season, a fifth basaltic meteorite LAP 03632 (0.09 kg) was found. On the basis of the oxygen isotope composition (McBride et al. 2003) and a preliminary petrographic examination during classification, McBride et al. (2003, 2004a, 2004b) concluded that the five stones are of lunar origin and are almost certainly paired with each other. Other investigators have studied the LAP meteorites and reached a similar conclusion (Collins et al. 2005; Day et al. 2005; Anand et al. 2004; Joy et al. 2005).On the basis of the work we present here for the LAP 02xxx stones, we find no reasons to dispute the hypothesis and many reasons to support it. In this paper, we use the designation LAP to refer collectively to the stones of the LaPaz Icefield basaltic lunar meteorite.

Here, we present the mineralogy, mineral chemistry, textures, and major- and trace-element composition of LAP. We infer from its composition that the parent melt for LAP had a composition similar to the low-Ti, yellow picritic glass of Apollo 15. We also show on the basis of composition and petrology that LAP is sufficiently similar to the lunar meteorite NWA 032 (Northwest Africa; Fagan et al. 2002) that the two meteorites are almost certainly source crater paired, i.e., that they were ejected from the Moon by a single impact.

SAMPLES STUDIED

We were allocated multiple chips of the five different LAP stones from different areas of the meteorite: LAP 02205,20 (258 mg), LAP 02205,24 (268 mg), LAP 02224,9 (122 mg), LAP 02224,19 (183 mg), LAP 02224,20 (181 mg), LAP 02226,6 (220 mg), LAP 02226,10 (111 mg), LAP 02226,12 (126 mg), LAP 02436,7 (120 mg), LAP 02436,9 (112 mg), LAP 02436,12 (135 mg), LAP 03632,7 (246 mg), and LAP 03632,13 (226 mg). We were also allocated polished thin sections LAP 02205,33 (surface area of ~1.5 cm^2), LAP 02224,24 (~0.6 cm^2), LAP 02226,16 (~1.1 cm^2), LAP

02436,14 (~0.6 cm^2), and LAP 03632,18 (~1.0 cm^2). For comparison, we present here compositional data for nine subsamples of basaltic lunar meteorite NWA 032. We collected the NWA 032 data under almost identical analytical conditions to those described below for LAP (see Fagan et al. 2002 for details). Previously, the chemical composition of NWA 032 has only been reported as mass-weighted averages (Fagan et al. 2002).

ANALYTICAL METHODS

We used a variety of analytical techniques to characterize the LAP samples. We obtained trace-element compositions by instrumental neutron activation analysis (INAA) and major-element compositions by a combination of INAA and electron microprobe analysis (EMPA) on fused beads. We characterized the textures and mineral assemblages with a combination of transmitted light and reflected light optical microscopy, as well as with backscattered electron imaging (BSE) using the electron microprobe. A combination of backscattered electron images and elemental X-ray maps were used to determine a mode for the thin sections. Finally, we characterized the mineral chemistry using EMPA.

For INAA, we subdivided each of the LAP 02205 chips into three ~40 mg subsamples, each of the LAP 02224, LAP 02226, and LAP 02436 chips into a single ~30 mg subsample, and each of the LAP 03632 chips into two ~35 mg subsamples. We sealed the samples in ultrapure silica tubing for neutron irradiation. The samples and multielement standards were irradiated in the research reactor of the University of Missouri—Columbia with a thermal neutron flux of 5.15×10^{13} $cm^{-2}s^{-1}$ for 24 hr. Radioassays were done using gamma ray spectrometry at 6, 7–9, 10–13, and 28–32 days following neutron irradiation. Several well-characterized rock and synthetic glasses were used as standards. Gamma-ray spectral data were reduced using the TEABAGS program (Lindstrom and Korotev 1982; Korotev 1991). INAA-derived compositional data are tabulated in Table 1.

We obtained data for mineral and glass compositions by EMPA using a JEOL 733 Superprobe with Advanced Microbeam Inc. automation. Mineral and glass analyses were conducted using wavelength dispersive spectrometers operating at 15 kV accelerating voltage and using a 20 nA beam current for feldspar and glass analyses, a 30 nA beam current for pyroxene and olivine analyses, and a 40 nA beam current for metal, oxide, and phosphate analyses. A set of oxide, mineral, and glass standards were used for calibration in WDS (wavelength dispersive spectroscopy) analyses. A spot size ranging from 1 to 10 μm was used for all mineral analyses. Count times varied depending on the target phase, but were typically about 10–30 sec on peak for major elements and 30–60 sec on peak for minor elements. The concentrations of Th and the rare earth elements (REEs) in phosphates were calibrated using ThO_2 and synthetic REE-orthophosphate standards (Jarosewich and Boatner 1991; Donavan et al. 2003), respectively, with count times of 90–120 sec. The detection limits for major and minor elements are ~0.02 wt%, and the detection limits for Th and the REEs ranged from 0.04 to 0.12 wt%. Data for mineral and glass compositions are reported in Tables 2–8.

For bulk major-element analysis, we ground each LAP 02xxx INAA subsample in an agate mortar and pestle after radioassay, and fused the resulting powder with a molybdenum strip resistance heater under an argon atmosphere (Jolliff et al. 1991). The LAP 03632 INAA subsamples were still too radioactive to handle so they were not analyzed at this time. We analyzed the resulting fused beads (FB) for major elements by EMPA using the previously described conditions, except that the spot size was increased to 40–50 μm and basaltic glass standards were used in addition to the mineral and oxide standards. Molybdenum concentrations averaged 0.08 wt% in the fused bead analyses and were almost always <0.3 wt%. Concentrations of Na_2O determined by EMPA were typically 5–10% lower (relatively) than INAA-derived concentrations. We attribute this discrepancy to systematic volatilization of Na_2O during the fusing process. Concentrations of FeO (i.e., total Fe as FeO) determined by EMPA on fused beads were typically 1–5% lower (relatively) than FeO concentrations determined by INAA. This is due to the incorporation of a small amount of Fe into the Mo metal during the fusing process. The whole-rock major-element concentrations tabulated in Table 1 are reported on a Mo-free basis. For FeO, Na_2O, and Cr_2O_3, the INAA-derived concentrations are reported because they are more accurate (Na, Fe) or precise (Cr). For the other major elements, values are normalized to yield the original EMPA oxides sum.

We determined modal mineral proportions by image analysis (4–9 million pixels per thin section) using a combination of BSE images and elemental X-ray maps for Mg, Al, Si, P, S, K, Ca, Ti, Cr, and Fe that covered the majority of each of the LAP 02xxx thin sections. The images were taken with a JEOL JSM840 scanning electron microscope. Results of modal analyses are tabulated in Table 9.

RESULTS

Petrography

The texture, mineral compositions, and mineral assemblages observed in the thin sections of the four LAP 02xxx stones are strongly alike (Fig. 1a–d). The petrographic description that follows is that of thin section LAP 02205,33 and is representative of all four sections. To demonstrate the similarity among the different LAP stones, we present mineral composition data for each of the 4 LAP 02xxx stones. Where one of the thin sections contains features that differ from those seen in LAP 02205,33, this is noted.

Table 1. Major- and trace-element concentrations of LAP 02205 and NWA 032 subsamples and weighted averages.

Sample	LAP 02205	LAP 02205	LAP 02205	LAP 02205	LAP 02205	LAP 02205	LAP 02224	LAP 02224	LAP 02224	LAP 02226	LAP 02226	LAP 02226	LAP 02436	LAP 02436	LAP 02436	LAP 03632
Split	,20-1	,20-2	,20-3	,24-1	,24-2	,24-3	,9-1	,19-1	,20-1	,6-1	,10-1	,12-1	,7-1	,9-1	,12-1	,7-1
Major-element concentrations																
SiO_2	45.0	45.3	45.2	45.3	44.7	45.2	45.3	45.0	45.7	45.8	45.6	45.7	45.8	45.4	44.9	–
TiO_2	3.34	3.33	3.34	2.99	3.28	3.13	2.98	3.33	2.65	3.23	3.19	3.22	2.81	2.74	2.77	–
Al_2O_3	9.84	10.18	10.48	9.63	8.98	10.20	10.40	9.35	9.76	9.50	9.78	9.16	10.67	9.37	9.37	–
Cr_2O_3 (INAA)	0.26	0.22	0.26	0.33	0.32	0.33	0.29	0.30	0.36	0.31	0.30	0.31	0.33	0.38	0.42	0.23
FeO (INAA)	22.9	22.8	21.9	21.7	23.3	21.6	22.7	23.1	21.5	21.8	21.7	21.9	20.9	21.8	22.8	21.8
MnO	0.28	0.30	0.29	0.28	0.34	0.32	0.26	0.28	0.28	0.28	0.28	0.29	0.25	0.28	0.27	–
MgO	5.87	5.46	5.69	7.17	7.11	6.68	5.76	6.56	7.49	6.72	6.45	7.10	6.30	7.93	7.74	–
CaO	11.1	11.2	11.4	11.1	10.5	11.3	11.2	10.9	11.1	11.1	11.4	11.1	11.4	11.0	10.5	–
Na_2O (INAA)	0.39	0.42	0.41	0.38	0.36	0.39	0.36	0.36	0.37	0.37	0.37	0.37	0.37	0.35	0.35	0.39
K_2O	0.08	0.09	0.07	0.06	0.07	0.06	0.10	0.08	0.06	0.06	0.07	0.06	0.08	0.05	0.06	–
P_2O_5	0.11	0.11	0.10	0.09	0.08	0.08	0.12	0.13	0.09	0.09	0.12	0.11	0.13	0.09	0.11	–
Totals	99.1	99.4	99.2	99.0	99.0	99.3	99.5	99.3	99.4	99.3	99.3	99.3	99.0	99.4	99.3	–
Mg′	31	30	32	37	35	36	31	34	38	35	35	37	35	39	38	–
Trace-element concentrations																
Sc	59.0	58.0	57.8	59.5	58.9	60.4	60.2	58.1	58.8	60.0	60.8	58.4	61.7	60.8	56.8	59.2
Cr	1751	1511	1767	2290	2180	2230	1982	2070	2470	2150	2040	2100	2240	2580	2840	1590
Co	34.6	33.9	34.0	37.8	40.4	37.0	38.5	37.1	38.5	35.5	35.0	37.8	34.3	41.5	42.7	31.5
Sr	150	160	190	130	130	110	140	140	130	140	140	100	130	130	130	100
Zr	200	260	250	210	150	140	130	190	190	180	150	220	190	100	170	200
Ba	166	154	150	124	134	152	153	163	144	144	157	142	139	86	126	157
La	14.7	15.3	14.2	11.6	15.3	14.6	12.5	14.5	11.4	11.8	12.7	12.4	11.0	10.6	11.8	13.6
Ce	38.3	39.6	36.6	32.2	37.0	36.0	33.6	38.8	30.8	32.9	34.5	34.4	31.9	27.3	31.6	36.9
Nd	25	28	23	20	27	20	22	25	16	18	26	24	18	20	19	22
Sm	8.60	8.89	8.35	7.04	8.51	8.19	7.48	8.61	6.84	7.24	7.62	7.42	6.80	6.32	7.05	8.13
Eu	1.36	1.41	1.36	1.20	1.26	1.29	1.21	1.30	1.12	1.19	1.25	1.22	1.20	1.02	1.14	1.28
Tb	1.89	2.02	1.91	1.63	1.95	1.86	1.73	2.03	1.66	1.68	1.77	1.73	1.67	1.51	1.65	1.85
Yb	7.3	7.4	7.0	6.1	7.0	6.7	6.5	7.3	6.0	6.2	6.6	6.4	5.9	5.3	6.1	7.0
Lu	0.99	1.03	0.96	0.83	0.95	0.94	0.91	1.00	0.82	0.87	0.91	0.90	0.84	0.73	0.86	1.00
Hf	6.27	6.42	6.06	5.10	5.71	5.50	5.67	6.33	5.04	5.25	5.65	5.49	5.01	4.18	5.19	5.97
Ta	0.80	0.80	0.79	0.69	0.67	0.69	0.74	0.80	0.61	0.70	0.73	0.75	0.63	0.57	0.63	0.76
Th	2.24	2.34	2.20	1.79	2.01	1.93	2.13	2.39	1.80	1.87	2.11	2.04	1.91	1.42	2.00	2.34
U	0.61	0.52	0.67	0.55	0.53	0.42	0.48	0.64	0.44	0.51	0.54	0.43	0.44	0.37	0.56	0.57
Mass (mg)	35.3	40.2	40.2	34.5	41.3	48.9	27.9	27.3	28.8	28.3	27.7	30.5	27.3	26.9	33.3	32.4

Table 1. *Continued.* Major- and trace-element concentrations of LAP 02205 and NWA 032 subsamples and weighted averages.

Sample	LAP 03632	LAP 03632	LAP 03632	NWA 032	NWA 032	NWA 032	NWA 032	NWA 032	NWA 032	NWA 032	NWA 032	NWA 032	LAP 032	NWA 032	LAP	NWA 032
Split	,7-2	,13-1	,13-2	A2	A3	A4	B1	B3	B4	C1	C2	D2	ave.	ave.	rsdev.	rsdev.
Major-element concentrations																
SiO_2	–	–	–	45.1	44.2	45.4	45.6	43.4	44.5	44.7	44.5	45.2	45.3	44.7	0.008	0.015
TiO_2	–	–	–	2.85	2.96	3.01	3.33	2.63	3.08	3.02	2.82	3.15	3.11	3.00	0.079	0.068
Al_2O_3	–	–	–	9.42	9.02	9.42	9.90	8.67	9.99	9.37	8.58	9.73	9.79	9.32	0.052	0.054
Cr_2O_3 (INAA)	0.33	0.31	0.28	0.40	0.37	0.37	0.36	0.42	0.39	0.56	0.36	0.38	0.31	0.40	0.156	0.154
FeO (INAA)	22.6	22.3	22.8	21.7	22.6	22.1	21.5	23.7	21.8	22.6	22.0	21.8	22.2	22.2	0.029	0.031
MnO	–	–	–	0.27	0.28	0.29	0.27	0.30	0.26	0.26	0.29	0.30	0.29	0.28	0.080	0.060
MgO	–	–	–	7.97	8.50	7.36	6.30	10.26	6.86	7.64	9.85	6.92	6.63	7.97	0.115	0.170
CaO	–	–	–	10.7	10.4	10.9	11.5	9.5	11.3	10.4	9.8	10.9	11.09	10.6	0.025	0.062
Na_2O (INAA)	0.37	0.38	0.37	0.36	0.34	0.35	0.38	0.33	0.37	0.32	0.34	0.35	0.38	0.35	0.050	0.052
K_2O	–	–	–	0.08	0.09	0.09	0.11	0.08	0.10	0.10	0.11	0.09	0.07	0.09	0.202	0.122
P_2O_5	–	–	–	0.08	0.08	0.06	0.10	0.07	0.08	0.11	0.11	0.10	0.10	0.09	0.158	0.208
Totals	–	–	–	99.0	98.9	99.3	99.3	99.3	98.8	99.1	98.8	98.9	99.28	99.0	–	–
Mg′	–	–	–	40	40	37	34	44	36	38	44	36	34.7	39	0.081	0.088
Trace-element concentrations																
Sc	58.5	60.4	59.1	60.8	53.7	58.0	57.9	49.6	55.1	50.7	54.4	58.4	59.2	55.2	0.021	0.067
Cr	2280	2100	1930	2760	2500	2500	2430	2870	2660	3800	2490	2600	2096	2760	0.156	0.154
Co	38.7	37.7	37.0	40.8	43.8	39.6	36.8	50.3	39.9	46.9	41.4	38.5	37.0	42.1	0.076	0.102
Sr	140	100	130	126	140	130	160	140	126	190	160	140	133	149	0.162	0.140
Zr	140	160	210	160	170	180	180	160	160	160	170	180	183	170	0.224	0.055
Ba	163	128	163	191	250	229	170	130	166	335	469	266	145	266	0.133	0.392
La	12.7	11.7	13.2	10.5	11.1	11.9	12.1	10.3	11.7	10.5	11.7	11.9	13.1	11.3	0.114	0.062
Ce	33.8	32.1	36.2	28.5	28.9	32.3	32.3	28.2	31.6	27.7	30.9	30.5	34.7	29.9	0.090	0.060
Nd	21	26	23	19	18	22	22	16	20	19	21	21	22	20	0.151	0.098
Sm	7.58	7.15	7.91	6.37	6.48	7.10	7.05	6.10	6.92	6.18	6.64	6.98	7.74	6.63	0.094	0.058
Eu	1.20	1.20	1.27	1.06	1.07	1.15	1.20	1.00	1.15	1.02	1.13	1.17	1.24	1.10	0.073	0.064
Tb	1.76	1.65	1.83	1.52	1.52	1.65	1.67	1.44	1.60	1.46	1.59	1.65	1.79	1.57	0.079	0.054
Yb	6.5	6.3	6.8	5.7	5.7	6.1	6.2	5.3	6.0	5.4	5.8	6.1	6.59	5.8	0.084	0.053
Lu	0.91	0.89	0.95	0.81	0.78	0.85	0.85	0.74	0.83	0.75	0.81	0.83	0.92	0.80	0.081	0.052
Hf	5.59	5.18	5.85	4.76	4.96	5.29	5.31	4.55	5.13	4.63	5.10	5.32	5.58	5.02	0.099	0.059
Ta	0.76	0.67	0.69	0.56	0.64	0.71	0.68	0.60	0.61	0.60	0.61	0.65	0.71	0.63	0.097	0.073
Th	1.96	1.96	2.17	1.74	1.91	1.99	2.04	1.67	1.96	1.72	1.87	2.03	2.04	1.89	0.114	0.074
U	0.42	0.55	0.59	0.35	0.44	0.44	0.45	0.39	0.40	0.51	0.57	0.49	0.52	0.46	0.158	0.144
Mass (mg)	34.1	37.3	38.8	9.0	21.0	8.1	10.7	9.6	7.7	18.2	15.6	24.2	641	124	–	–

Major-element concentrations in wt% and trace-element concentrations in ppm. Major elements not otherwise labeled were obtained by EMPA on fused beads made from the same INAA split. Averages (ave.) are weighted averages; rsdev. = relative standard deviation. The relative uncertainties in the INAA data are: 1–2% for Na_2O, Sc, Cr, Co, FeO, La, Ce, Sm, Yb, Lu, and Hf; 3–4% for Eu, Tb, and Th; 7–10% for Ta and Ba; 17% for U; and 25–30% for Sr and Zr.

Table 2. Average and representative olivine compositions in the LAP basaltic meteorites.

	LAP 02205 core	LAP 02226 core	LAP 02224 core	LAP 02436 core	LAP 02205 t-rim	LAP 02226 t-rim	LAP 02224 t-rim	LAP 02436 t-rim	LAP 02205 x-rim	LAP 02224 x-rim	LAP 02436 x-rim	LAP 02205 fay. symp.
N	40	24	63	29	42	17	10	5	4	1	2	2
Major elements in wt% by EMPA												
SiO_2	35.92	36.01	35.90	36.28	34.54	34.24	34.09	34.21	31.40	30.43	31.15	29.72
TiO_2	0.04	0.04	0.04	0.04	0.06	0.06	0.04	0.08	0.11	0.52	0.10	0.34
Al_2O_3	0.03	0.09	0.02	0.03	<0.02	<0.02	0.05	<0.02	<0.02	<0.02	<0.02	<0.02
Cr_2O_3	0.24	0.21	0.23	0.22	0.17	0.16	0.11	0.06	0.07	0.06	0.03	<0.02
FeO	34.44	32.92	32.82	33.14	42.06	40.15	41.75	45.70	58.63	62.85	58.79	66.50
MnO	0.33	0.36	0.35	0.36	0.47	0.41	0.42	0.50	0.63	0.71	0.58	0.65
MgO	28.26	29.24	30.12	29.63	22.46	23.50	22.55	19.30	8.81	4.61	8.44	1.77
NiO	<0.05	n.a.	n.a.	n.a.	<0.05	n.a.	n.a.	n.a.	n.a.	n.a.	n.a.	n.a.
CaO	0.35	0.34	0.36	0.33	0.33	0.36	0.35	0.36	0.45	0.53	0.54	0.55
Na_2O	<0.02	<0.02	<0.02	<0.02	<0.02	<0.02	<0.02	<0.02	0.02	<0.02	<0.02	<0.02
Total	99.65	99.22	99.85	100.03	100.16	98.90	99.37	100.22	100.12	99.71	99.65	99.55
Cation ratios												
Fa	40.6	38.7	38.0	38.6	51.4	49.0	51.1	57.1	78.7	88.4	79.6	95.0
Fo	59.4	61.3	62.0	61.4	48.7	51.0	48.9	42.9	21.1	11.6	20.4	4.5
Stoichiometry based on 4 oxygen atoms												
Si IV	0.999	0.998	0.989	0.997	0.995	0.992	0.990	1.003	0.995	0.995	0.994	0.996
Al VI	0.001	0.003	0.001	0.001	0.000	0.000	0.002	0.000	0.000	0.000	0.000	0.000
Ti VI	0.001	0.001	0.001	0.001	0.001	0.001	0.001	0.002	0.003	0.013	0.002	0.009
Cr	0.005	0.005	0.005	0.005	0.004	0.004	0.003	0.001	0.002	0.002	0.001	0.000
Fe^{+2}	0.801	0.764	0.756	0.762	1.016	0.973	1.016	1.122	1.554	1.719	1.569	1.864
Mn^{+2}	0.008	0.009	0.008	0.008	0.012	0.010	0.010	0.012	0.017	0.020	0.016	0.018
Mg	1.171	1.208	1.236	1.214	0.962	1.014	0.974	0.842	0.416	0.225	0.401	0.089
Ca	0.011	0.010	0.011	0.010	0.010	0.011	0.011	0.011	0.015	0.018	0.019	0.020
Na	0.000	0.000	0.000	0.000	0.000	0.000	0.001	0.000	0.001	0.000	0.000	0.000
Tet site	0.999	0.998	0.989	0.997	0.995	0.992	0.990	1.003	0.995	0.995	0.994	0.996
Oct site	1.998	1.999	2.019	2.001	2.006	2.014	2.017	1.991	2.007	1.996	2.009	1.999

N = number of analyses in the average; t-rim = typical rim; x-rim = extreme rim; fay. symp. = fayalite symplectite; n.a. = not analyzed.

Table 3. Average and representative pyroxene compositions in the LAP basaltic meteorites.

	LAP 02205 pig. core	LAP 02226 pig. core	LAP 02224 pig. core	LAP 02436 pig. core	LAP 02205 aug. core	LAP 02226 aug. core	LAP 02224 aug. core	LAP 02436 aug. core	LAP 02205 hd.	LAP 02436 hd.	LAP 02205 pyxfer.
N	23	14	17	16	8	20	14	11	1	1	1
Major elements in wt% by EMPA											
SiO_2	51.67	51.94	52.07	51.83	49.51	49.27	49.46	49.51	45.60	45.91	43.97
TiO_2	0.56	0.51	0.53	0.56	1.35	1.35	1.30	1.34	1.39	1.85	1.12
Al_2O_3	1.33	1.20	1.32	1.36	3.17	3.33	3.24	3.28	1.84	2.05	1.73
Cr_2O_3	0.59	0.54	0.58	0.54	0.97	1.01	0.94	0.98	<0.02	<0.02	<0.02
FeO	19.84	19.47	19.16	19.83	13.86	13.21	13.32	13.77	31.21	30.66	47.18
MnO	0.36	0.35	0.36	0.35	0.25	0.25	0.26	0.27	0.32	0.33	0.59
MgO	18.81	19.20	19.63	18.52	13.47	13.81	14.05	13.80	0.48	0.33	0.04
CaO	6.39	6.49	6.38	6.82	16.81	16.96	16.74	16.58	17.88	18.37	3.53
Na_2O	<0.02	0.03	0.03	0.02	0.05	0.05	0.06	0.05	<0.02	<0.02	0.02
Total	99.57	99.73	100.1	99.82	99.44	99.23	99.35	99.57	98.73	99.51	98.17
Cation ratios											
Mg′	62.8	63.7	64.6	62.5	63.4	65.1	65.3	64.1	2.6	1.9	0.1
Fs	31.7	31.0	30.4	31.6	24.9	23.7	23.7	24.6	58.2	58.0	87.1
En	53.6	14.6	14.2	15.7	43.1	32.1	31.7	31.3	40.2	40.9	0.1
Wo	14.7	54.4	55.4	52.6	32.0	44.2	44.6	44.0	1.6	1.1	12.8
Stoichiometry based on 6 oxygen atoms											
Si IV	1.949	1.953	1.948	1.952	1.883	1.874	1.878	1.879	1.916	1.908	1.933
Al IV	0.051	0.047	0.052	0.048	0.117	0.126	0.122	0.121	0.084	0.092	0.066
Ti IV	0.000	0.000	0.000	0.000	0.000	0.000	0.000	0.000	0.000	0.000	0.000
Al VI	0.009	0.006	0.006	0.012	0.026	0.023	0.023	0.026	0.007	0.008	0.009
Ti VI	0.016	0.014	0.015	0.016	0.038	0.039	0.037	0.038	0.044	0.058	0.054
Cr	0.018	0.016	0.017	0.016	0.029	0.030	0.028	0.029	0.000	0.000	0.000
Fe^{+2}	0.626	0.612	0.599	0.624	0.441	0.420	0.423	0.437	1.097	1.066	1.734
Mn^{+2}	0.011	0.011	0.011	0.011	0.008	0.008	0.008	0.009	0.011	0.012	0.022
Mg	1.058	1.076	1.094	1.039	0.764	0.783	0.795	0.781	0.030	0.021	0.002
Ca	0.258	0.261	0.256	0.275	0.685	0.691	0.681	0.674	0.805	0.818	0.166
Na	0.001	0.002	0.002	0.001	0.003	0.004	0.004	0.004	0.001	0.001	0.002
Tet site	2.000	2.000	2.000	2.000	2.000	2.000	2.000	2.000	2.000	2.000	1.999
Oct site	1.997	1.999	2.001	1.995	1.995	1.999	2.001	1.997	1.995	1.983	1.989

Augite (aug.) cores have an Mg′ >60 and Wo >30, while pigeonite (pig.) cores have Mg′ >60 and Wo <18. Hd. = hedenbergite; pyxfer. = pyroxferroite. Mg′ = Mg/(Mg + Fe)*100. N = number of analyses.

All of the LAP stones have relatively coarse-grained (up to approximately 1.5 mm) subophitic texture. They consist predominantly of pyroxene and plagioclase, with minor amounts of olivine, ilmenite, and a groundmass dominated by fayalite and cristobalite. They contain trace amounts of chromite, chromian ulvöspinel, ulvöspinel, troilite, Fe-metal, barian K-feldspar, fluor-apatite, RE-merrillite, tranquillityite ($Fe_8(Y,Zr)_2Ti_3Si_3O_{24}$), and baddeleyite ($ZrO_2$). The modal mineral proportions differ slightly from section to section (Table 9). A few veins and pockets of basaltic glass of pseudo-whole rock composition (likely shock melted) also occur in thin sections LAP 02205,33 and LAP 02224,24. The order in which minerals are inferred to have crystallized is chromite, olivine, pyroxene, plagioclase, and groundmass.

Olivine grains vary in size from 0.03 to ~1 mm, with 0.1 to 0.3 mm being typical. The modal abundance of olivine ranges from 2.3% to 3.6%. The grains are usually anhedral (rarely subhedral; Fig. 2a), typically with round or irregular morphology and uneven contact with the surrounding pyroxene (Fig. 2b). Some olivine grains have inclusions of chromite or Cr-ulvöspinel grains or both, and a few have "melt" inclusions that have two phases in them: mafic glass with a pyroxene-like composition (~10 wt% Al_2O_3; Table 6) and K-rich, high-silica glass similar to the glass seen in the fayalite symplectite grains in the groundmass (~3 wt% K_2O, 68 wt% SiO_2). Most of the larger olivine grains are zoned, with cores of $Fo_{55–65}$ and rims typically in the $Fo_{38–45}$ range (Fig. 3a; Table 2), though in a few instances zoning to rims of $Fo_{\sim 20}$ is observed (Fig. 3b). Most of the smaller olivine grains are not zoned (or not strongly zoned), and they typically have compositions in the $Fo_{52–57}$ range, with the smallest grains having the most magnesian compositions. The apparent reaction texture between olivine and pyroxene and the relatively magnesian rims on compositions of the smallest olivine grains (likely the remnant cores of grains that have been almost completely resorbed) are strong indications that olivine was being resorbed when the rock solidified.

Chromite and Cr-ulvöspinel grains almost always occur as inclusions within or closely associated with olivine grains. They also have relatively restricted compositional ranges (Fig. 4; Table 4), and they occur individually and as composite grains with cores of chromite ($Chr_{62–68}Usp_{13–18}Spn_{16–25}$) and rims of Cr ulvöspinel ($Chr_{6–19}Usp_{71–91}Spn_{3–11}$) (Figs. 5a and 5b). We found few spinel compositions intermediate to these end members. The total modal abundance of spinel (including ulvöspinel in the groundmass) is small, ranging from 0.3 to 0.4%. Where these two phases are intergrown, the boundary between them is sharp, with differences in Cr_2O_3 concentration exceeding 20 wt% within a few micrometers of the boundary. A few of the chromite grains have inclusions of pyroxene with a range of compositions (Mg′ of 47–59, $Wo_{16–31}$, and TiO_2 concentrations from 1.1–2.4 wt%).

Pyroxene grains in LAP are anhedral, display undulatory to mosaic extinction, and range in size up to ~1 mm (Fig. 2c). In many cases, pyroxene grains partially enclose plagioclase grains in a subophitic texture. The modal abundance of pyroxene ranges from 47% to 52%. The pyroxene grains have magnesian cores of pigeonite and subcalcic augite (Mg′ from ~50 to 68), with a wide range of CaO concentrations (Wo_{11} to Wo_{36}; Table 3; Fig. 6), although there appears to be a bimodal distribution of Wo contents with a minimum near Wo_{20} (Fig. 6, insets). In some cases, pyroxene core compositions grade continuously to nearly end member hedenbergite ($Fs_{58}Wo_{40}$) and pyroxferroite ($Fs_{86}Wo_{13}$). In a few rare cases, contacts between magnesian and ferroan pyroxenes are sharp and linear. Compositions of pyroxene grains in contact with partially resorbed olivine grains vary considerably in composition. The most common composition is subcalcic augite (Wo > 20) with FeO concentrations in the range $Fs_{24–49}$.

The Ti/Al and Ti/Cr ratios in the LAP pyroxenes are strongly correlated with Mg′, as expected according to element compatibility (e.g., Bence and Papike 1972). The atomic Ti/Cr ratio increases with decreasing Mg′ in LAP pyroxenes (Fig. 7a). This reflects the compatible behavior of Cr and the incompatible behavior of Ti in early crystallizing phases of low-Ti lunar basaltic magmas. The most magnesian pyroxenes have atomic Ti/Al ratios very close to 1/4, indicating that aluminum was introduced through both the Tschermak ($AlAlMg_{-1}Si_{-1}$) and coupled titanium ($TiAl_2Mg_{-1}Si_{-2}$) exchange reactions in approximately equal proportions (Thompson 1982). As pyroxene becomes progressively more ferroan, the Ti/Al cation ratio approaches 1/2, suggesting a gradual increase in the proportion of Al incorporated due to coupled Ti substitution (Fig. 7b). The least magnesian pyroxenes (Mg′ <40) have Ti/Al ratios approaching 3/4. An increase in Ti/Al ratios in pyroxene from 1/4 to 1/2 with decreasing Mg′ in lunar basalts has previously been interpreted as a result of pyroxene crystallization both prior to the onset of plagioclase crystallization (ratios around 1/4) and during plagioclase crystallization (1/4–1/2; Bence and Papike 1972). Bence and Papike (1972) attributed the high relative concentrations of Ti in the late-stage, Fe-rich lunar pyroxenes to Ti^{3+}.

Plagioclase forms elongated, subhedral to anhedral grains up to 1.75 mm long. The modal abundance of plagioclase ranges from 32% to 35%. Pyroxene inclusions of a variety of sizes, with compositions spanning nearly the entire compositional spectrum observed, occur within plagioclase. Most plagioclase grains are highly fractured, although some, or portions of some, are smooth in polished sections, as seen in the BSE images (Fig. 2d). These smooth areas consist partially or entirely of maskelynite, as indicated by their isotropic (or nearly isotropic) character in cross-polarized light. Plagioclase grains are complexly zoned. Their typical core composition is $An_{88.6}Ab_{11}Or_{0.4}$, with ~1 wt% FeO + MgO, and an Mg′ of 34 (Fig. 8; Table 5). Their rims are as wide as ~40 μm and gradually increase in K (up to ~Or_5)

Table 4. Average oxide compositions in the LAP basaltic meteorites.

	LAP 02205 Al chr.	LAP 02226 Al chr.	LAP 02224 Al chr.	LAP 02436 Al chr.	LAP 02205 Cr-rich usp.	LAP 02226 Cr-rich usp.	LAP 02224 Cr-rich usp.	LAP 02436 Cr-rich usp.	LAP 02205 Cr,Al usp.	LAP 02226 Cr,Al usp.	LAP 02224 Cr,Al usp.
N	23	11	13	5	22	16.00	7	13	9	22	10
Major elements in wt% by EMPA											
FeO	34.44	35.03	35.32	34.33	57.05	58.32	58.46	58.68	61.91	61.98	61.80
TiO_2	5.46	5.32	5.40	5.17	28.33	28.71	28.92	29.09	32.54	31.51	31.61
Cr_2O_3	43.84	43.57	43.31	43.91	9.28	8.40	8.51	7.76	2.34	3.10	3.38
Al_2O_3	11.42	11.78	11.40	12.17	2.87	2.61	2.61	2.76	1.91	2.04	2.03
MgO	2.83	2.42	2.18	2.92	0.93	0.61	0.69	0.65	0.21	0.28	0.31
MnO	0.27	0.24	0.25	0.27	0.35	0.32	0.34	0.33	0.36	0.32	0.34
V_2O_3	0.73	0.74	0.76	0.75	0.36	0.31	0.33	0.33	0.22	0.25	0.26
SiO_2	0.07	0.09	0.08	0.09	<0.02	0.07	0.08	0.18	<0.02	0.08	0.07
CaO	0.04	0.04	0.03	<0.02	0.10	0.05	0.06	0.11	0.08	0.07	0.05
ZnO	0.03	n.a.	n.a.	n.a.	0.04	n.a.	n.a.	n.a.	0.03	n.a.	n.a.
Totals	99.1	99.2	98.7	99.6	99.3	99.4	100.0	99.9	99.6	99.6	99.9
Stoichiometry based on 4 (spinel) and 3 (ilmenite) oxygen atoms											
Si IV	0.003	0.003	0.003	0.003	0.000	0.003	0.003	0.006	0.000	0.003	0.003
Al VI	0.469	0.484	0.472	0.496	0.125	0.114	0.113	0.119	0.083	0.089	0.088
Ti	0.143	0.139	0.143	0.134	0.784	0.798	0.798	0.803	0.907	0.880	0.880
V	0.020	0.021	0.021	0.021	0.011	0.009	0.010	0.010	0.007	0.007	0.008
Cr	1.208	1.201	1.204	1.199	0.270	0.245	0.247	0.225	0.068	0.091	0.099
Fe^{2+}	1.004	1.021	1.039	0.992	1.756	1.802	1.794	1.801	1.920	1.925	1.913
Mn^{2+}	0.008	0.007	0.007	0.008	0.011	0.010	0.011	0.010	0.011	0.010	0.011
Mg	0.147	0.126	0.114	0.151	0.051	0.034	0.038	0.035	0.012	0.016	0.017
Zn	0.001	–	–	–	0.001	–	–	–	0.001	–	–
Ca	0.002	0.002	0.001	0.000	0.004	0.002	0.002	0.004	0.003	0.003	0.002
Sum 2+	1.162	1.156	1.161	1.151	1.823	1.847	1.844	1.851	1.947	1.953	1.942
Sum 3, 4+	1.844	1.849	1.844	1.854	1.190	1.168	1.170	1.163	1.066	1.071	1.078
Total	3.003	3.001	3.002	3.001	3.012	3.013	3.012	3.007	3.013	3.020	3.017

and FeO (up to ~3 wt%), while decreasing in MgO (to <0.02 wt%; Fig. 9). The Na_2O concentrations first increase up to ~Ab_{14}, then decrease sharply to less than Ab_{10} (which is lower than in the cores). The extreme rim composition of the large plagioclase grains is similar to that of the plagioclase found as inclusions in groundmass fayalite and cristobalite grains (next paragraph; Table 5). There is no apparent overall compositional difference between the cores of the maskelynite and the plagioclase grains.

Fayalite, cristobalite, and ilmenite are the dominant minerals in the groundmass, typically occurring together, although each can be found independently. All of the phases have relatively minor modal abundances: fayalite (2.9–4.8%), cristobalite (1.8–2.1%), and ilmenite (3.5–4.0%). Silica displaying the "crackle" pattern distinctive to cristobalite, occurs as anhedral grains up to 0.5 mm in size. The cristobalite grains contain minor Al_2O_3, TiO_2, FeO, and CaO (Σ ~1.3 wt%; Table 6). Inclusions of late-crystallizing phases such as K-rich plagioclase, K-rich glass, K-feldspar, fayalite, Fe-rich pyroxene, phosphate, and mafic glass with high concentrations of incompatible elements are common (Fig. 5c). Fayalite grains ($Fo_{4.5}$; ~0.5 wt% CaO) range in size up to 0.75 mm and usually form a symplectite texture with inclusions of K-rich glass, silica, K-rich plagioclase, and ilmenite (Fig. 5d). Fayalite with no (or few) inclusions occurs only rarely. Ilmenite is the dominant oxide in the groundmass, forming elongate laths up to 1 mm in length. Typically the ilmenite is poor in Mg (~0.2 wt% average), although a single grain of more magnesian ilmenite associated with a large olivine grain was observed (Fig. 2b). Less common are smaller subhedral ulvöspinel grains (<0.05 mm) that have compositions approaching end member ulvöspinel ($Chr_{0–4}Usp_{93–98}Sp_{2–3}$). A few composite grains of ilmenite and ulvöspinel were observed.

Also found in the groundmass are a variety of trace minerals, including both fluorapatite and RE-merrillite (Table 7). Phosphate grains most commonly occur between plagioclase and ferropyroxene, sometimes with associated cristobalite, troilite, or both. Barian K-feldspar (~5 wt% BaO) also occurs in the groundmass, usually in the same areas as the phosphate minerals (Table 5). Only a few K-feldspar grains (the largest) have stoichiometry that unambiguously identifies them as K-feldspar, while many K-rich grains have excess Si, suggesting that they may be intergrowths of

Table 4. *Continued.* Average oxide compositions in the LAP basaltic meteorites.

	LAP 02436 Cr,Al usp.	LAP 02205 end usp.	LAP 02226 end usp.	LAP 02224 end usp.	LAP 02436 end usp.	LAP 02205 ilm.	LAP 02226 ilm.	LAP 02224 ilm.	LAP 02436 ilm.	LAP 02205 Mg ilm.
N	11	11	2	3	3	24	16	20	18	2
Major elements in wt% by EMPA										
FeO	62.02	63.75	64.45	63.55	64.65	46.57	46.47	46.34	46.24	44.63
TiO_2	33.53	32.67	32.26	33.96	32.31	51.98	52.26	52.33	52.64	52.96
Cr_2O_3	2.09	0.26	0.23	0.11	0.37	0.10	0.12	0.15	0.16	0.38
Al_2O_3	2.02	1.79	2.06	2.16	2.27	0.08	0.11	0.13	0.10	0.06
MgO	0.22	0.05	0.08	0.07	0.03	0.14	0.10	0.16	0.19	1.50
MnO	0.34	0.31	0.27	0.29	0.27	0.38	0.33	0.37	0.27	0.35
V_2O_3	0.23	0.18	0.15	0.19	0.16	0.31	0.29	0.29	0.28	0.35
SiO_2	0.15	<0.02	0.11	0.10	0.07	0.03	0.03	0.24	0.04	<0.02
CaO	0.07	0.10	0.07	0.08	0.10	0.13	0.06	0.10	0.09	0.08
ZnO	n.a.	0.08	n.a.	n.a.	n.a.	0.03	n.a.	n.a.	n.a.	<0.02
Totals	100.7	99.2	99.7	100.5	100.2	99.7	99.8	100.1	100.0	100.3
Stoichiometry based on 4 (spinel) and 3 (ilmenite) oxygen atoms										
Si IV	0.005	0.001	0.004	0.004	0.003	0.001	0.001	0.006	0.001	0.000
Al VI	0.087	0.079	0.091	0.093	0.099	0.002	0.003	0.004	0.003	0.002
Ti	0.920	0.921	0.906	0.937	0.901	0.990	0.993	0.989	0.996	0.991
V	0.007	0.005	0.004	0.006	0.005	0.006	0.006	0.006	0.006	0.007
Cr	0.060	0.008	0.007	0.003	0.011	0.002	0.002	0.003	0.003	0.007
Fe^{2+}	1.893	1.999	2.012	1.950	2.005	0.986	0.982	0.974	0.973	0.928
Mn^{2+}	0.010	0.010	0.009	0.009	0.009	0.008	0.007	0.008	0.006	0.007
Mg	0.012	0.003	0.004	0.004	0.002	0.005	0.004	0.006	0.007	0.056
Zn	–	0.002	–	–	–	0.001	–	–	–	0.000
Ca	0.003	0.004	0.003	0.003	0.004	0.004	0.002	0.003	0.002	0.002
Sum 2+	1.918	2.018	2.028	1.966	2.019	1.004	0.995	0.991	0.988	0.994
Sum 3, 4+	1.080	1.014	1.012	1.043	1.019	1.001	1.005	1.008	1.009	1.007
Total	2.992	3.032	3.035	3.005	3.036	2.004	2.000	1.992	1.996	2.001

The spinel catagories where chosen based primarily on Cr_2O_3 content, with Al chromite (chr.) having >40 wt% Cr_2O_3, Cr-rich ulvöspinel (usp.) having 15–5 wt% Cr_2O_3, Cr,Al ulvöspinel having 5–0.5 wt% Cr_2O_3, and endmember ulvospinel having <0.5 wt% Cr_2O_3. Also seen were Ti,Al chromite (30–40 wt% Cr_2O_3) and high-Cr ulvöspinel (30–15 wt% Cr_2O_3), which are likely the result of an anlyses overlapping simultaneously on both an Al chromite and Cr-rich ulvöspinel grain. Similarly, compositions intermediate to ilmenite and end ulvöspinel were seen. These compositions are not listed in this table but are shown in Fig. 4. N = number of analyses in the average; n.a. = not analyzed.

K-feldspar and silica (granophyric texture) at a scale small enough to be beyond the resolution of the electron microprobe (less than ~0.1 μm).

Two glass types of distinct composition, presumably late-stage residual liquids, occur in the groundmass. The first is a K,Si-rich glass (78 wt% SiO_2, ~5.6 wt% K_2O) that makes up a considerable percentage of the inclusions in the cristobalite and particularly the fayalite grains. The second type of evolved glass occurs as very small (<5 μm) rounded inclusions in cristobalite grains. This glass has a silica-poor, Fe-rich bulk composition (~36 wt% SiO_2, ~39 wt% FeO; Table 6), but it is also considerably enriched in many incompatible elements: 2.3 wt% P_2O_5, 1.2 wt% SO_3, 0.2 wt% Y_2O_3). Commonly, we observed minute grains of fayalite, troilite, or phosphate associated with this glass. These two late-stage glasses could represent conjugate liquids produced by late-stage immiscibility of an evolved residual melt. Similar glasses were observed in some plutonic rocks from the Apollo 14 site (Jolliff et al. 1991).

Troilite blebs (with nearly ideal stoichiometry; Table 8) are scattered throughout the groundmass along with trace Fe-metal grains, which are usually intergrown with troilite or overgrown on chromite grains. These grains typically contained 6.6 wt% Ni and 1.4 wt% Co, though one grain had 33.8 wt% Ni and 6.0 wt% Co (Table 8). A few grains of baddelyite (ZrO_2) and tranquillityite (Zr-Fe-Ti silicate) were identified by energy-dispersive spectroscopy (EDS) in the groundmass.

A variety of shock effects occur in the minerals of these thin sections (e.g., plagioclase converted to maskelynite, mosaicism in the pyroxene). The level of shock was such that localized partial melting occurred in some areas of the meteorite. The areas of shock melt have several morphologies: small melt pockets (LAP 02205; Fig 10a), veins of melt (LAP 02224,24; Fig. 10b), and in some cases, areas that were only partially melted (LAP 02224,24; Fig. 10c) with discernable mineral grains still present (typically maskelynite). Although veins of shock melt are rare

Table 5. Average and representative feldspar compositions in the LAP basaltic meteorites.

	LAP 02205 plag. core	LAP 02226 plag. core	LAP 02224 plag. core	LAP 02436 plag. core	LAP 02205 mask. core	LAP 02226 mask. core	LAP 02224 mask. core	LAP 02436 mask. core	LAP 02205 plag. Na rim	LAP 02226 plag. Na rim
N	123	86	48	88	29	49	33	32	12	3
Major elements in wt% by EMPA										
SiO_2	47.15	46.57	46.89	46.39	47.53	47.41	46.63	46.73	49.49	49.60
TiO_2	0.10	0.07	0.07	0.06	0.13	0.08	0.06	0.06	0.27	0.19
Al_2O_3	33.37	33.67	32.96	33.63	33.67	32.91	33.76	34.15	31.70	31.03
Cr_2O_3	0.03	<0.02	<0.02	0.02	0.07	0.02	<0.02	0.02	0.04	0.03
FeO	0.68	0.67	0.73	0.58	0.60	1.11	0.66	0.60	1.34	1.36
MgO	0.23	0.22	0.17	0.24	0.27	0.29	0.28	0.29	0.08	0.12
CaO	17.30	17.46	17.09	17.63	17.47	17.26	17.30	17.40	16.28	15.97
BaO	n.a.	n.a.	n.a.	n.a.	n.a.	n.a.	n.a.	n.a.	n.a.	n.a.
Na_2O	1.20	1.23	1.36	1.21	1.19	1.23	1.31	1.28	1.48	1.53
K_2O	0.06	0.07	0.10	0.06	0.05	0.09	0.06	0.05	0.20	0.19
Total	100.0	100.0	99.4	99.8	100.8	100.4	100.1	100.6	100.6	100.0
Cation ratios										
An	88.5	88.3	86.9	88.7	88.8	88.1	87.7	88.0	84.8	84.2
Or	0.4	0.4	0.6	0.4	0.3	0.5	0.3	0.3	1.2	1.2
Ab	11.1	11.2	12.5	11.0	10.9	11.3	12.0	11.7	14.0	14.6
Cn	0.0	0.0	0.0	0.0	0.0	0.0	0.0	0.0	0.0	0.0
Stoichiometry based on 8 oxygen atoms										
Si IV	2.168	2.147	2.173	2.143	2.168	2.179	2.147	2.140	2.259	2.279
Al IV	1.809	1.830	1.801	1.831	1.810	1.782	1.832	1.843	1.705	1.681
Fe^{+2}	0.026	0.026	0.028	0.023	0.023	0.043	0.025	0.023	0.051	0.052
Mg	0.016	0.015	0.011	0.017	0.019	0.020	0.019	0.020	0.005	0.008
Ca	0.853	0.863	0.849	0.872	0.854	0.850	0.853	0.854	0.796	0.786
Ba	–	–	–	–	–	–	–	–	–	–
Na	0.107	0.110	0.122	0.108	0.105	0.109	0.117	0.114	0.131	0.136
K	0.004	0.004	0.006	0.004	0.003	0.005	0.003	0.003	0.011	0.011
Tet. site	3.977	3.977	3.974	3.974	3.978	3.961	3.979	3.984	3.964	3.960
Oct. site	1.005	1.018	1.022	1.023	1.003	1.027	1.022	1.013	0.995	0.994

in our thin sections, such veins were reported as pervasive in the original macroscopic description of all five LAP stones (McBride et al. 2003, 2004a, 2004b).

The various shock-induced effects observed in LAP can be used to quantify and constrain the level of shock that LAP experienced. The presence of both plagioclase and maskelynite in these samples suggests that the lower end of the range listed for conversion of plagioclase to maskelynite (30–45 GPa; Stöffler and Hornemann 1972; Ostertag 1983) is appropriate. The mosaicism seen in the pyroxene is typically associated with shock values in the 30–75 GPa range (Kieffer et al. 1976; Schaal et al. 1979). The presence of shock-melt veins that have melted both pyroxene and plagioclase (based on the melt composition; Table 6) indicates LAP should have been subjected to shock levels of >75–80 GPa (Kieffer et al. 1976; Schaal et al. 1979). The different shock effects observed reflect a range from <30 GPa (areas were plagioclase is preserved) to >75 GPa (areas where shock melting occurred) over distances of only a few millimeters.

Bulk Composition and Comparison to Other Lunar Basalts

LAP is a moderately aluminous (~10 wt% Al_2O_3), low-Ti (3.1 wt% TiO_2) mare basalt that falls near the Fe-rich (22.2 wt% FeO) end of the range of FeO concentrations observed among lunar basalts. It is more ferroan (Mg′ = 34.7) than any basalt in the Apollo or Luna collection (Fig. 11a). Among lunar basalts, only meteorites Asuka-881757 and Yamato-793169 have comparably low Mg′ values (Koeberl et al. 1993; Warren and Kallemeyn 1993; Thalmann et al. 1996; Korotev et al. 2003a). LAP is enriched in Na_2O (0.38 wt%) relative to other ferroan (e.g., Asuka-881757 and Yamato-793169) and Fe-rich basalts, except for NWA 032 (Fig. 11b).

Regarding trace elements, LAP is enriched in Co compared to most lunar mare basalts with comparable Sc concentrations (Table 1; Fig. 12a). Among Apollo and Luna basalts, only the Apollo 12 ilmenite basalts (Rhodes et al. 1977; Neal et al. 1994) are comparable. Incompatible trace-

Table 5. *Continued.* Average and representative feldspar compositions in the LAP basaltic meteorites.

	LAP 02224 plag. Na rim	LAP 02436 plag. Na rim	LAP 02205 plag. matrix	LAP 02205 plag. K rim	LAP 02226 plag. K rim	LAP 02224 plag. K rim	LAP 02436 plag. K rim	LAP 02205 barian K-spar.	LAP 02205 K,Ba glass	LAP 02205 K,Ba glass
N	24	5	13	10	1	5	1	10	10	23
Major elements in wt% by EMPA										
SiO_2	49.01	48.79	51.22	51.52	48.88	49.35	50.17	60.26	59.35	63.56
TiO_2	0.08	0.08	0.16	0.17	<0.02	0.08	0.14	n.a.	n.a.	n.a.
Al_2O_3	31.63	31.20	29.60	29.93	32.13	30.04	30.02	20.19	20.63	20.43
Cr_2O_3	0.02	0.02	0.06	0.05	<0.02	0.03	<0.02	n.a.	n.a.	n.a.
FeO	1.17	1.30	2.67	1.92	1.47	1.95	1.73	0.65	0.74	1.16
MgO	0.06	0.09	0.03	0.02	<0.02	<0.02	0.02	<0.02	<0.02	0.10
CaO	16.20	16.22	15.20	15.49	16.18	16.02	15.60	0.63	0.66	2.07
BaO	n.a.	n.a.	n.a.	n.a.	n.a.	n.a.	n.a.	5.01	4.07	3.72
Na_2O	1.57	1.55	1.05	1.05	1.32	1.26	1.50	0.31	0.29	0.33
K_2O	0.23	0.21	0.90	0.67	0.67	0.56	0.86	13.54	11.62	5.86
Total	100.0	99.5	100.7	100.6	100.7	99.3	100.0	100.8	100.6	100.7
Cation ratios										
An	83.9	84.2	84.6	85.2	83.5	84.5	80.7	3.3	–	–
Or	1.4	1.3	6.1	4.4	4.1	3.5	5.3	84.2	–	–
Ab	14.7	14.5	10.5	10.4	12.4	12.0	14.0	3.0	–	–
Cn	0.0	0.0	0.0	0.0	0.0	0.0	0.0	9.6	–	–
Stoichiometry based on 8 oxygen atoms										
Si IV	2.253	2.257	2.342	2.344	2.237	2.293	2.312	2.863	2.864	2.951
Al IV	1.714	1.701	1.596	1.609	1.732	1.645	1.631	1.131	1.173	1.124
Fe^{+2}	0.045	0.050	0.102	0.073	0.056	0.076	0.067	0.026	0.030	0.045
Mg	0.004	0.006	0.002	0.001	0.000	0.001	0.001	0.001	0.001	0.007
Ca	0.798	0.804	0.745	0.757	0.793	0.798	0.770	0.032	0.034	0.100
Ba	–	–	–	–	–	–	–	0.093	0.077	0.070
Na	0.140	0.139	0.093	0.093	0.117	0.113	0.134	0.029	0.027	0.029
K	0.013	0.013	0.052	0.039	0.039	0.033	0.050	0.820	0.715	0.353
Tet. site	3.967	3.957	3.938	3.954	3.969	3.938	3.943	3.994	4.037	4.075
Oct. site	0.013	1.011	0.995	0.963	1.007	1.020	1.022	1.002	0.884	0.604

Plag. = plagioclase; mask. = maskelynite; N = number of analyses in the average; n.a. = not analyzed.

element concentrations are considerably greater in LAP than in most of other low-Ti basalts (Fig. 12b–c), including the Apollo 12 ilmenite basalts (Haskin et al. 1971; Neal et al. 1994). The exceptions are NWA 032, the high-Al basalts of Luna 16 (Philpotts et al. 1972; Helmke and Haskin 1972; Ma et al. 1979), and some Apollo 14 high-Al basalts (Dickinson et al. 1985; Shervais et al. 1985; Neal et al. 1989a, 1989b).

Relative concentrations of REEs in the LAP basalt are also dissimilar to those of most other lunar basalts (Fig. 13) in that LAP is enriched in light REEs. The exceptions are NWA 032, which has a pattern nearly parallel to LAP, and Apollo 14 group 3 basalts (Dickinson et al. 1985), which have a pattern that is similar although somewhat less steep in the heavy REEs. Ratios of Th to REE in LAP are higher than those of all other lunar basalts except NWA 032 (Fig. 14), and the disparity in Th/REE ratio between LAP and other lunar basalts (except NWA 032) increases from the light to heavy REEs. The Apollo 14 high-K basalts have similar Th/REE ratios for the middle REE Sm-Tb, however (Neal et al. 1989a, 1989b). Overall, in terms of its trace-element concentrations, LAP 02205 is most similar to NWA 032. The main differences are that NWA 032 is richer in elements associated with olivine (Mg, Cr, Co) and has concentrations of incompatible elements that are 78–91% as great as those in LAP 02205.

DISCUSSION

Evidence Supporting the Lunar Origin and Pairing of the LAP Stones

As stated in the introduction, the meteorites LAP 02205, 02224, 02226, 02436, and 03632 were identified as lunar basalts that were almost certainly paired (McBride et al. 2003, 2004a, 2004b). A brief summary follows of the attributes found in our more detailed petrographic examination that support this initial classification and pairing interpretation.

Results of oxygen isotope analyses ($\delta^{18}O$ = +5.6 and

Table 6. Average and representative cristobalite and glass composition in the LAP basaltic meteorites.

	LAP 02205 cristobalite	LAP 02226 cristobalite	LAP 02224 cristobalite	LAP 02436 cristobalite	LAP 02205 Si-rich MI glass	LAP 02205 pyx-like MI glass	LAP 02205 K glass in sympl.	LAP 02205 ITE-rich mafic glass	LAP 02205 shock glass area	LAP 02224 shock glass area	LAP 02224 shock glass vein
N	6	2	5	4	4	1	2	5	1	65	15
Major elements in wt% by EMPA											
SiO_2	97.95	98.17	98.47	98.45	67.25	42.76	78.32	36.67	46.3	48.6	44.1
TiO_2	0.27	0.27	0.23	0.23	0.66	4.81	0.37	4.03	2.34	1.62	3.13
Al_2O_3	0.73	0.60	0.64	0.78	18.79	9.42	10.13	5.44	13.9	8.6	12.3
Cr_2O_3	0.02	<0.02	<0.02	0.02	<0.02	0.13	<0.02	<0.02	0.08	0.38	0.28
FeO	0.21	0.40	0.19	0.17	1.86	15.91	1.83	39.27	19.6	18.5	20.5
MnO	n.a.	n.a.	n.a.	n.a.	n.a.	0.22	n.a.	0.42	0.22	0.29	0.25
MgO	0.02	<0.02	<0.02	<0.02	0.33	8.17	<0.02	0.21	3.45	9.85	7.17
CaO	0.19	0.20	0.20	0.23	6.89	19.16	0.98	9.76	12.7	11.8	11.4
BaO	n.a.	n.a.	n.a.	n.a.	1.17	n.a.	n.a.	n.a.	n.a.	n.a.	n.a.
Na_2O	0.13	0.10	0.09	0.12	0.62	0.11	0.19	0.06	0.51	0.36	0.49
K_2O	0.03	0.05	0.07	<0.02	1.67	n.a.	5.66	0.30	0.05	n.a.	n.a.
P_2O_5	n.a.	n.a.	n.a.	n.a.	n.a.	n.a.	n.a.	2.32	n.a.	n.a.	n.a.
F	n.a.	n.a.	n.a.	n.a.	n.a.	n.a.	n.a.	0.08	n.a.	n.a.	n.a.
Y_2O_3	n.a.	n.a.	n.a.	n.a.	n.a.	n.a.	n.a.	0.19	n.a.	n.a.	n.a.
Ce_2O_3	n.a.	n.a.	n.a.	n.a.	n.a.	n.a.	n.a.	0.12	n.a.	n.a.	n.a.
SO_3	n.a.	n.a.	n.a.	n.a.	n.a.	n.a.	n.a.	1.23	n.a.	n.a.	n.a.
Total	99.55	99.80	99.90	100.0	99.24	100.70	97.49	100.2	99.1	100.0	99.6

Sympl. = symplectite, MI = melt inclusion, N = number of analyses in the average, n.a. = not analyzed. The shocked glass in LAP 02224 is the partially melted area (see Fig. 14), and only the anaylses of the glass itself were included in the average not the minerals that were analyzed.

Table 7. Representative phosphate compositions in LAP 02205,33.

	LAP 02205 RE-merrillite	LAP 02205 RE-merrillite	LAP 02205 RE-merrillite	LAP 02205 RE-merrillite	LAP 02205 RE-merrillite	LAP 02205 fluorapatite	LAP 02205 fluorapatite	LAP 02205 fluorapatite
Major elements in wt% by EMPA								
SiO_2	0.50	0.44	0.62	0.37	3.21	2.28	4.49	1.37
Al_2O_3	0.22	<0.05	0.09	<0.05	<0.05	0.07	0.14	<0.05
FeO	6.37	7.74	5.68	5.76	2.50	1.69	4.39	2.02
MgO	0.20	0.37	0.25	0.28	<0.05	<0.05	<0.05	<0.05
CaO	43.26	40.35	42.33	42.45	49.83	52.41	50.03	53.51
Na_2O	0.00	0.01	0.10	0.14	0.00	0.00	0.01	0.00
P_2O_5	38.85	41.71	43.82	43.60	35.40	39.49	37.71	40.77
Cl	<0.05	<0.05	<0.05	<0.05	<0.05	0.06	0.27	0.31
F	0.47	0.44	0.50	0.48	1.68	2.45	1.30	1.86
Y_2O_3	2.98	2.93	2.26	2.21	1.72	1.03	0.78	0.53
La_2O_3	0.93	1.07	0.65	0.64	0.92	0.24	0.14	0.12
Ce_2O_3	2.53	2.59	1.89	1.85	2.53	0.72	0.69	0.53
Nd_2O_3	1.61	1.77	1.08	1.18	1.66	0.57	0.59	0.31
Sm_2O_3	0.43	0.43	0.29	0.28	0.48	0.22	0.15	0.09
Gd_2O_3	0.87	0.90	0.58	0.58	0.79	0.23	0.18	0.08
Yb_2O_3	0.16	0.32	0.09	<0.05	0.10	0.05	<0.05	<0.05
ThO_2	0.07	0.09	0.08	<0.05	0.21	<0.05	<0.05	<0.05
–O = (F,Cl)	0.21	0.20	0.22	0.21	0.72	1.05	0.61	0.85
Sums	99.30	101.0	100.1	99.68	100.4	100.5	100.3	100.6

Table 8. Average sulfide and metal compositions in LAP 02205,33.

	Ave. Fe metal	High-Ni metal	Troilite
N	5	1	8
Elemental percentage by EMPA			
Fe	92.09	58.80	62.80
Ni	6.64	33.77	<0.02
Co	1.41	5.95	<0.02
Ti	0.23	0.09	0.06
Cr	0.43	0.17	<0.02
Mn	<0.02	0.04	<0.02
S	<0.02	<0.02	36.20
Totals	100.8	98.8	99.4

Ideal troilite = 36.5 wt% S, 63.5 wt% Fe. N = number of analyses.

Table 9. Modal mineralogy of the different LAP stones.

	LAP 02205,33	LAP 02226,16	LAP 02224,24	LAP 02436,14
Pyroxene	51.5	50.5	46.9	46.6
Plagioclase	31.9	32.1	32.3	34.6
Ilmenite	3.48	3.91	3.86	3.99
Fay. sympl.	3.09	2.90	3.58	4.83
Olivine	2.33	2.71	3.63	3.20
Cristobalite	2.14	2.09	1.78	2.00
Spinel (all)	0.34	0.45	0.40	0.39
Troilite	0.25	0.24	0.24	0.22
Fractures	4.9	4.9	5.3	4.21
Shock glass	0.1	0.2	2.2	0.0
N	6.33×10^6	9.05×10^6	4.70×10^6	3.96×10^6

All modal values are listed as percentages. N = number of pixels.

Fig. 1. Backscattered electron (BSE) images of the different thin sections of LAP. The brightest phases are ilmenite (elongate) and fayalite (more equant), the darkest grey phase is cristobalite, the dark grey, typically elongate phase is plagioclase and the medium grey phases are pyroxene and olivine. a) LAP 02226,16. b) LAP 02436,14. c) LAP 02224,24. d) LAP 02205,33.

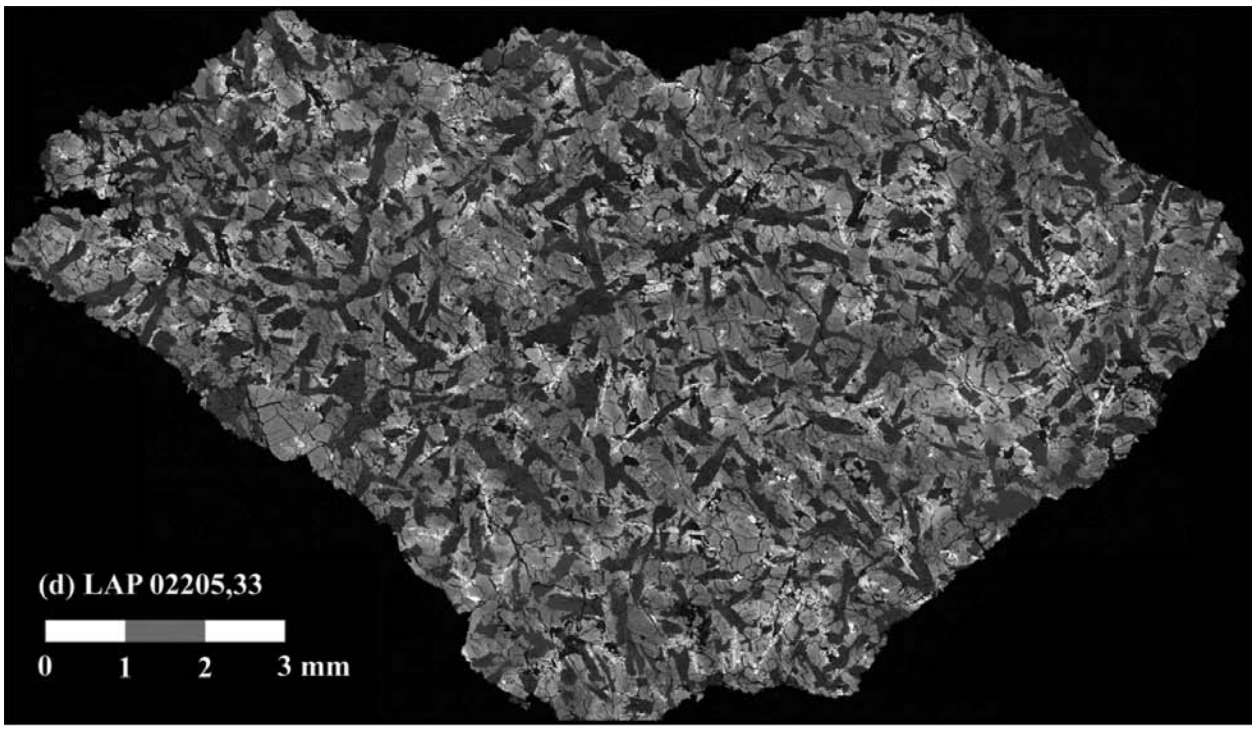

Fig. 1. *Continued.* Backscattered electron (BSE) images of the different thin sections of LAP. The brightest phases are ilmenite (elongate) and fayalite (more equant), the darkest grey phase is cristobalite, the dark grey, typically elongate phase is plagioclase and the medium grey phases are pyroxene and olivine. d) LAP 02205,33.

$\delta^{17}O = +2.7$) performed by Mayeda and Clayton (reported in McBride et al. 2003) constrain the origin of LAP 02205 to the Earth, the Moon, or an enstatite meteorite parent body. LAP is clearly a meteorite; all four of the stones have fusion crusts (ruling out a terrestrial origin). The extremely ferroan nature of LAP rules out the enstatite parent body as the provenance. FeO/MnO ratios of mafic silicates are diagnostic of origins from different planetary bodies in the solar system (Dymek et al. 1976; Papike 1998). Ratios of FeO/MnO in LAP pyroxenes (average ~60) and olivines (average ~95) are consistent only with lunar origin (Fig. 15). Furthermore, the presence of Fe(Ni) metal and troilite, the completely anhydrous nature of the sample, the apparent lack of Fe^{3+} in all phases, the calcic nature of the plagioclase, and the deep negative Eu anomaly are all common in lunar basalts.

With regard to texture, mineral assemblage, and mineral chemistry, the four LAP 02xxx stones appear to be indistinguishable from each other. Although we did not study the mineral chemistry of the LAP 03632 in depth, the texture and mineral assemblage are identical to the LAP 02xxx stones. Furthermore, the collection locations of the five stones form a linear array ~3 km in length that is perpendicular to the flow of the ice sheet (John Schutt, personal communication). Thus, in the absence of cosmic-ray exposure data to the contrary, we conclude that the four LAP 02xxx stones studied are paired.

Compositional Variability among Small Subsamples of LAP 02205 and NWA 032

Samples of lunar meteorites available for study, at most a few hundred milligrams, are very small by the standards of terrestrial geology and geochemistry. Nevertheless, we have taken our samples and subdivided them into numerous, even smaller (10–50 mg) subsamples for bulk compositional analysis (Korotev et al. 1983, 1996, 2003a, 2003b; Jolliff et al. 1991, 1998; Fagan et al. 2002). This procedure provides an estimate of the whole-rock composition through a mass-weighted mean that is equivalent to a single analysis of the entire mass of the allocated sample. The variation among small subsamples, however, provides additional information about compositional variations associated with mineral assemblage and proportions, about petrogenesis, and about possible relationships to other meteorites (e.g., Korotev et al. 2003a, 2003b), and how well the "whole-rock" composition is likely to represent that of the source region of the meteorite (Korotev et al. 2000a). In the following discussion, we evaluate the causes of differences in composition among small subsamples of LAP and NWA 032.

The range of concentrations among the 19 subsamples of LAP (27–40 mg) is relatively small for the most precisely determined major elements (SiO_2, TiO_2, Al_2O_3, FeO, CaO, Na_2O) and most precisely determined trace elements that are compatible with the major mineral phases (Co, Sc, Eu), The

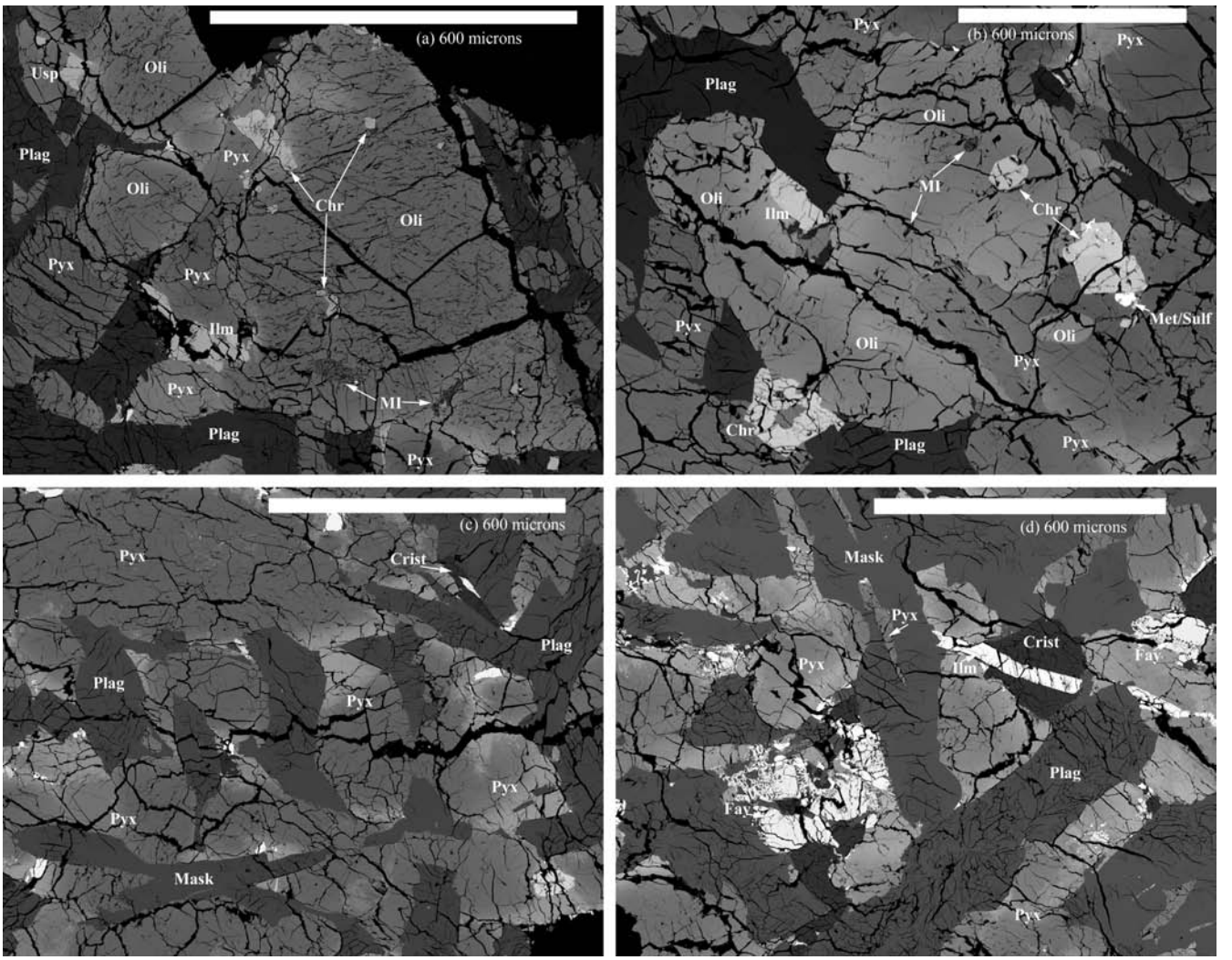

Fig. 2. BSE images from LAP 02205,33: a) a large, round olivine (oli) grain and a smaller subhedral olivine grain (left center of the image), both surrounded by zoned pyroxene (pyx) and plagioclase (plag), with melt inclusions (MI) and inclusions of chromite (chr). A small ulvöspinel (Usp) grain occurs in the upper left. b) A large irregular olivine grain and a smaller, mostly resorbed olivine grain. The larger grain contains both melt inclusions (MI) and chromite grains. The associated ilmenite (Ilm) grain is the most magnesian ilmenite grain observed. A composite grain of metal and troilite (Met/Sulf) is also present. c) A BSE image showing the zoning in multiple large pyroxene grains intergrown with plagioclase and maskelynite (mask) grains. One small cristobalite (crist) grain is also present. d) A BSE image showing several large plagioclase grains, some of which contain both fractured areas (plagioclase) and smooth areas (maskelynite). Also present are several areas of groundmass, including a fayalite symplectite and a cristobalite grain cut by an ilmenite lath.

relative sample standard deviations ($s/\bar{x}$) range from 0.8 to 7.6% (with only Co and Eu > 5%; Table 1). The exceptions are MgO and Cr_2O_3, for which the relative standard deviations are distinctly greater: 12% and 16%, respectively. For incompatible elements that we determined precisely (<9% analytical uncertainty: La, Ce, Sm, Tb, Yb, Lu, Hf, Ta, and Th), relative standard deviations range from 7 to 11%. These variations are caused by a combination of unrepresentative sampling of the major mineral phases, owing to the coarse grain size (up to ~1 mm^3) relative to the INAA subsample size (about 12 mm^3 assuming that the density of LAP is ~3.5 g/mm^3), and to the heterogeneous distribution of some relatively minor phases with high concentrations of a given element. This problem is not new, as many investigators have previously wrestled with the problem of studying relatively coarse-grained lunar basalts with small allocated subsample sizes characteristic of rare extraterrestrial samples (Korotev and Haskin 1975; Haskin et al. 1977; Lindstrom and Haskin 1978; Ryder and Schuraytz 2001). Ryder and Schuraytz (2001) showed that ~5 g of material are needed to achieve a representative sample of Apollo 15 olivine-normative basalts, which have grain sizes on the order of a millimeter or greater.

Among the LAP subsamples, Cr_2O_3 and MgO concentrations correlate positively ($R^2 = 0.81$), as a result of the association of chromite and Cr-ulvöspinel with olivine.

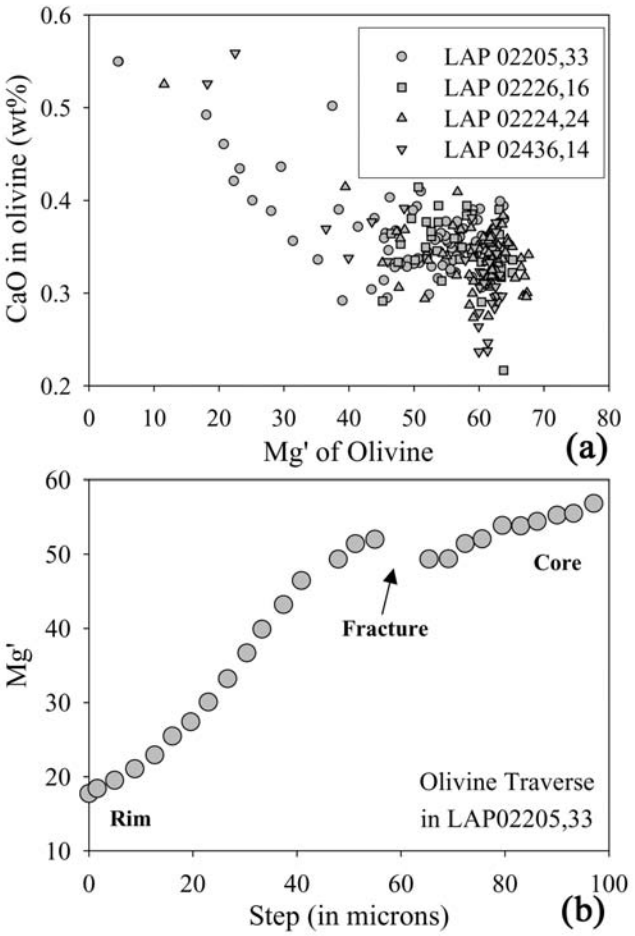

Fig. 3. a) CaO versus Mg′ (molar Mg/[Mg + Fe]*100) in the olivines of the different LAP stones. The compositions range from cores of $Fo_{55–67}$ trending towards rims typically in the Fo_{40} range, with extreme zonation to rims of $Fo_{15–20}$ in a few cases. Where analyzed, the composition of groundmass fayalite are also shown. b) An electron microprobe traverse across a small strongly zoned olivine grain in LAP 02205,33. The grain shows zoning from a core of ~Fo_{58} to a rim composition of ~Fo_{18} over ~100 μm. The break in the zoning (black arrow) is centered on a fracture in the olivine grain.

The large variations seen in MgO, Cr_2O_3 and, to a lesser extent, Co concentrations occur because of the large relative variation in the fraction of modal olivine among the subsamples. Normatively, the compositional range corresponds to −0.3–2.5 % olivine (one subsample has 0.3% normative quartz) and 0.32–0.49% chromite. The relatively small variations seen among concentrations of the other major elements, as well as Sc and Eu, are controlled by unrepresentative sampling of the major mineral phases pyroxene (Sc, Ca, Fe, Si) and plagioclase (Al, Na, Ca, Si, Eu), and the minor but widely distributed mineral ilmenite (Ti, Fe). Trace amounts of a few minerals that are found only in groundmass have high concentrations of incompatible trace elements relative to the concentration of those elements in the bulk meteorite. These minerals include K-feldspar (Ba),

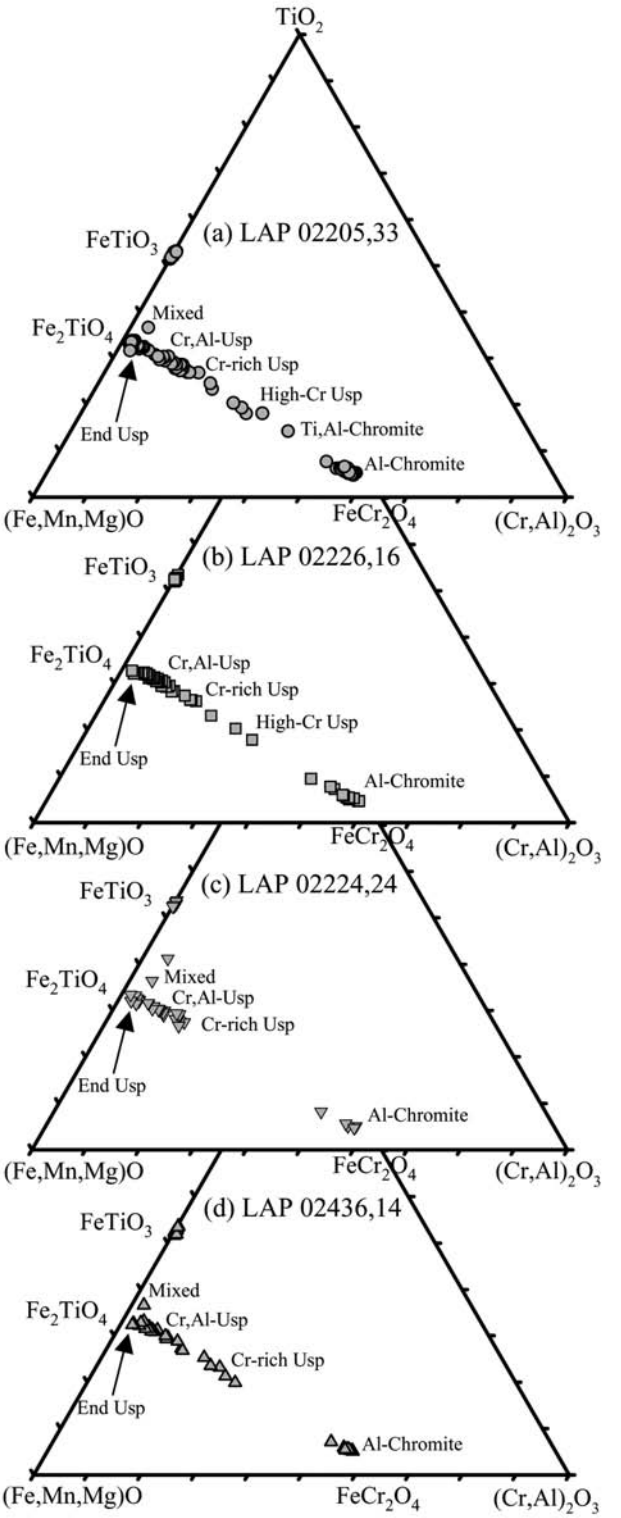

Fig. 4. Compositions of LAP oxides plotted on the (Fe,Mg,Mn)O-$(Cr,Al)_2O_3$-TiO_2 ternary (after El Goresy et al. 1971). Compositions of endmember ilmenite ($FeTiO_3$), ulvöspinel (Fe_2TiO_4), and chromite ($FeCr_2O_4$) are labeled. For a description of the classification scheme, see the footnote of Table 3. a) LAP 02205,33. b) LAP 02226,16. c) LAP 02224,24. d) LAP 02436,14.

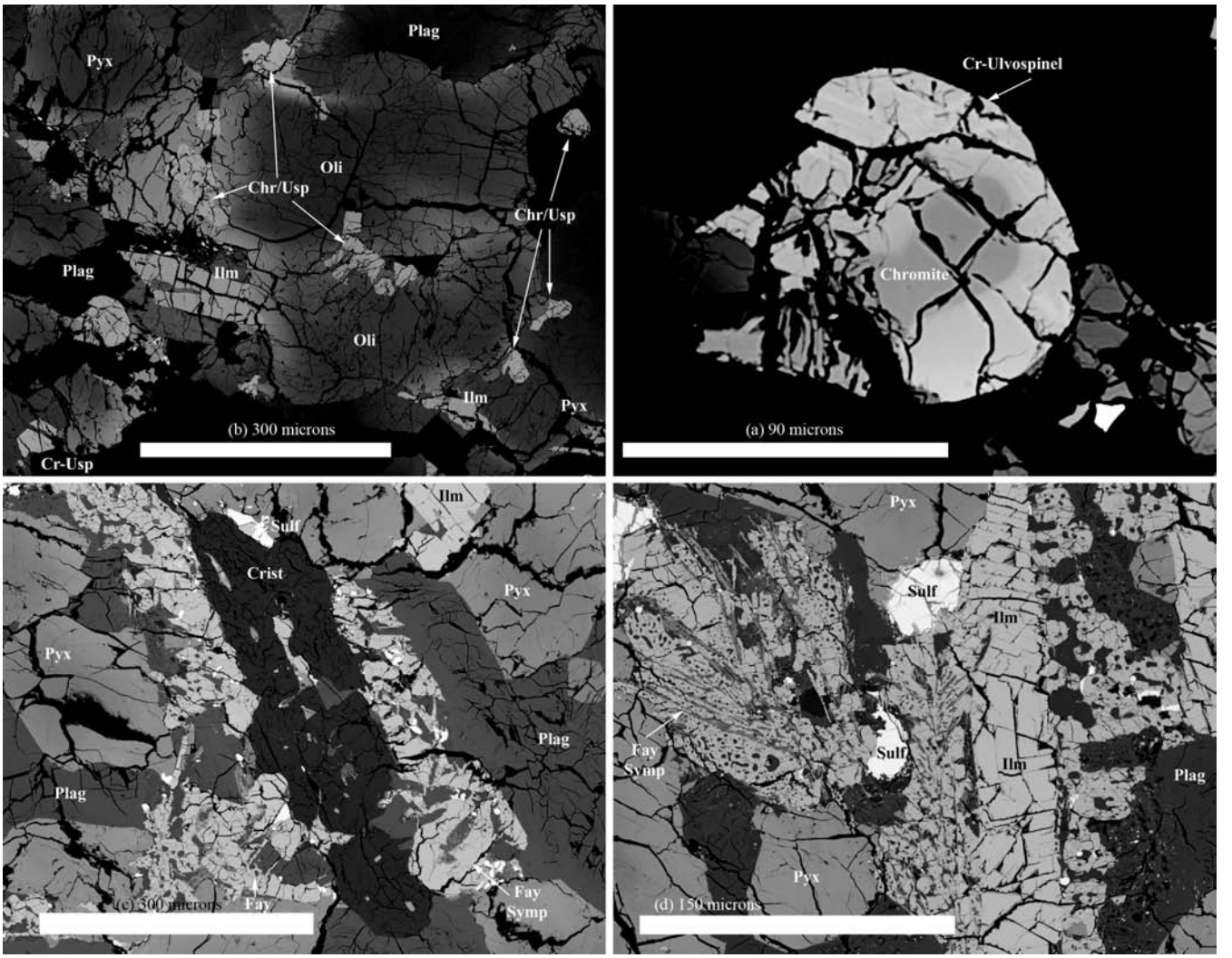

Fig. 5. BSE images from LAP 02205,33: a) oxide grains set in and around a large olivine grain; individual grains of ilmenite (Ilm), Cr-ulvöspinel (Chr-Usp), and chromite (Chr); composite chromian ulvöspinel-chromite (Chr/Usp) grains with accompanying pyroxene and plagioclase (grey and black areas). b) A close-up of a zoned spinel grain with a chromite core and a Cr-ulvöspinel rim. c) A large cristobalite (Crist) grain with many inclusions of fayalite, pyroxene (Pyx), plagioclase (Plag), troilite (Sulf), phosphate, K-rich glass, and the ITE-rich glass. Also present are several areas of fayalite symplectite (Fay Symp) with inclusions of plagioclase, silica, ilmenite, troilite, and K-rich glass. d) A BSE image of a different area of groundmass showing a large grain of fayalite symplectite containing inclusions of plagioclase, silica, ilmenite, troilite, K-rich glass, and Fe-rich pyroxene. A large ilmenite (Ilm) grain cuts through the symplectite, and several large troilite grains are also present.

RE-merrillite (P, REEs, Th), and baddeleyite (Zr, Hf, U, Th). Therefore, the variation in the amount of the groundmass "phase" in the different subsamples controls the ITE concentrations in the various subsamples.

For most of the major elements, subsamples of NWA 032 have relative standard deviations (RSD) that are insignificantly different from those of LAP (Table 1) even though the average subsample size for NWA 032 (~14 mg; Fagan et al. 2002) was smaller than for LAP (~34 mg). The RSDs of MgO and Cr_2O_3 for NWA 032 are again high because it has a porphyritic texture with large phenocrysts (millimeter scale) of olivine (with chromite inclusions) and magnesian pyroxene, but a fine-grained groundmass of plagioclase, Fe-rich pyroxene, ilmenite, and glass keeps the RSDs of other major and incompatible trace elements low.

Source Crater Pairing of LAP and NWA 032

We find the similarities in chemistry and petrography between LAP and NWA 032, when compared to the large ranges observed among Apollo and Luna samples, to be so great that it is highly unlikely that two meteorites so similar could derive from different locations. Below, we summarize the similarities and differences.

The textures of NWA 032 and LAP are markedly different from each other. NWA 032 has a porphyritic texture

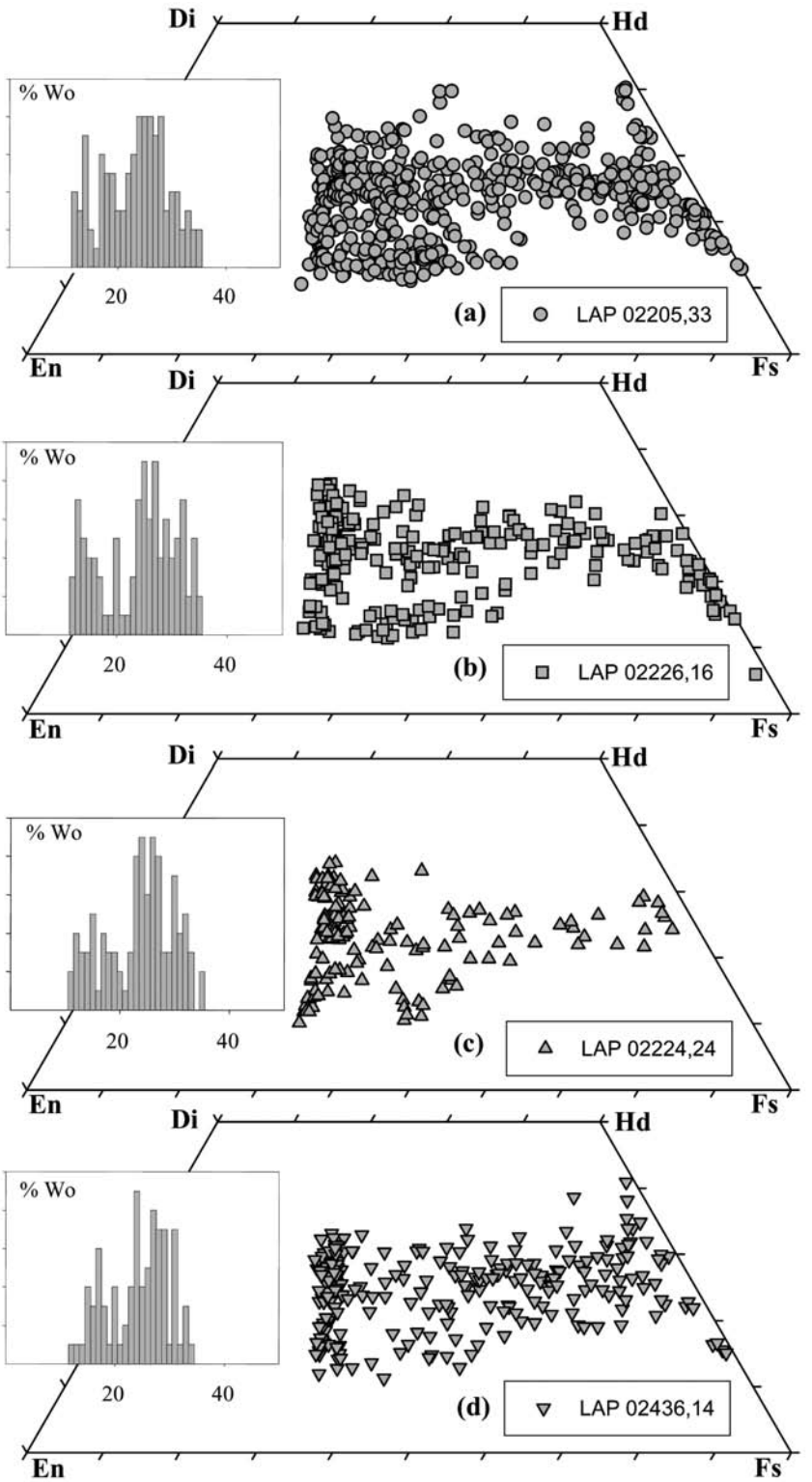

Fig. 6. Pyroxene quadrilaterals showing the composition of the zoned pyroxenes in the LAP meteorites. The patterns are very similar in all four stones. The cores of the zoned pyroxenes are magnesian ($Mg_{55–68}$) and are zoned continuously towards rim compositions that approach hedenbergite and pyroxferroite. The insets in each quadrilateral show the histogram of Wo contents in pyroxene analyses with an Mg′ between 50 and 70. A gap, or at least the hint of a gap, is seen at ~Wo_{20} in all four stones. a) LAP 02205,33. b) LAP 02226,16. c) LAP 02224,24. d) LAP 02436,14.

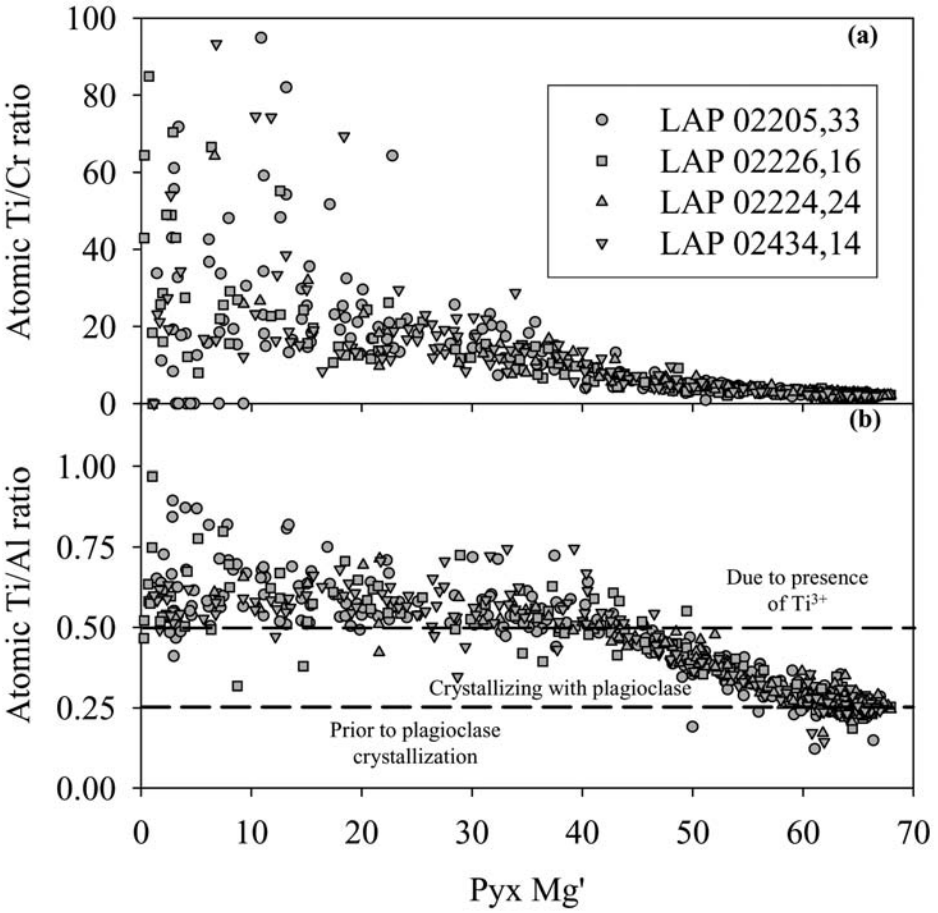

Fig. 7. a) Molar Ti/Cr ratio versus Mg′ in LAP pyroxenes. All four stones show a similar trend. The Ti/Cr ratio increases with decreasing Mg′, likely as a result of early chromite crystallization depleting the residual magma in Cr. b) Ti/Al ratio versus Mg′ in LAP 02205.33 pyroxenes. The pattern is essentially identical for all four stones. The Ti/Al ratio increases from ~0.25 to ~0.5 with decreasing Mg′, likely as a result of plagioclase crystallization. The high Ti/Al ratios seen in the most ferroan pyroxenes suggest the presence of Ti^{3+}, which alters the substitution patterns (see text for more detail).

(with a crystalline groundmass), indicating a relatively short period of slow cooling followed by rapid cooling (but not quenching). LAP has a subophitic texture with minerals that zone to extreme end member compositions, indicative of slow, steady cooling over an extended period of time. Textural differences such as these by themselves do not preclude a petrogenetic relationship between LAP and NWA 032 because such differences can occur within a single basalt flow. For example, the Elephant Mountain basalt flow in the Columbia River basalt province varies from ~15% crystalline at the top of the flow to >80 % crystalline near the center of the flow, and this is only a 10 m thick basalt flow (Schmincke 1967).

The mineral assemblages and mineral compositions of NWA 032 and LAP are very similar to each other. The olivine in both meteorites has compositions ranging from ~Fo_{20} to ~Fo_{65}. The olivine grains in both meteorites, contain melt inclusions with identical morphologies (although no compositional data is yet published on the olivine melt inclusions for NWA 032). Pyroxenes in NWA 032 and LAP cover a similar compositional range. In both meteorites they have magnesian cores (Mg′ 50–70) of pigeonite and subcalcic augite, although NWA 032 pyroxene cores are slightly more calcic and less magnesian. Ferroan pyroxene approaching pyroxferroite is found in both meteorites as well, with hedenbergite seen in LAP but not reported by Fagan et al. (2002) in NWA 032 (Fig. 16). The ranges in plagioclase composition in NWA 032 ($An_{80–90}$) and LAP ($An_{79–91}$) are similar. The oxide mineral assemblages in both samples are similar, with early chromite associated with the olivine grains, followed by later Mg-poor ilmenite and nearly end member ulvöspinel. The match is not exact, however, as LAP also has Cr-ulvöspinel. The Fe,Ti-oxides in NWA 032 also have higher concentrations of Al_2O_3, MgO, CaO, and SiO_2 than LAP, likely as a consequence of more rapid crystallization in NWA 032.

On nearly any two-element variation diagram for lithophile elements, subsamples of NWA 032 and LAP plot

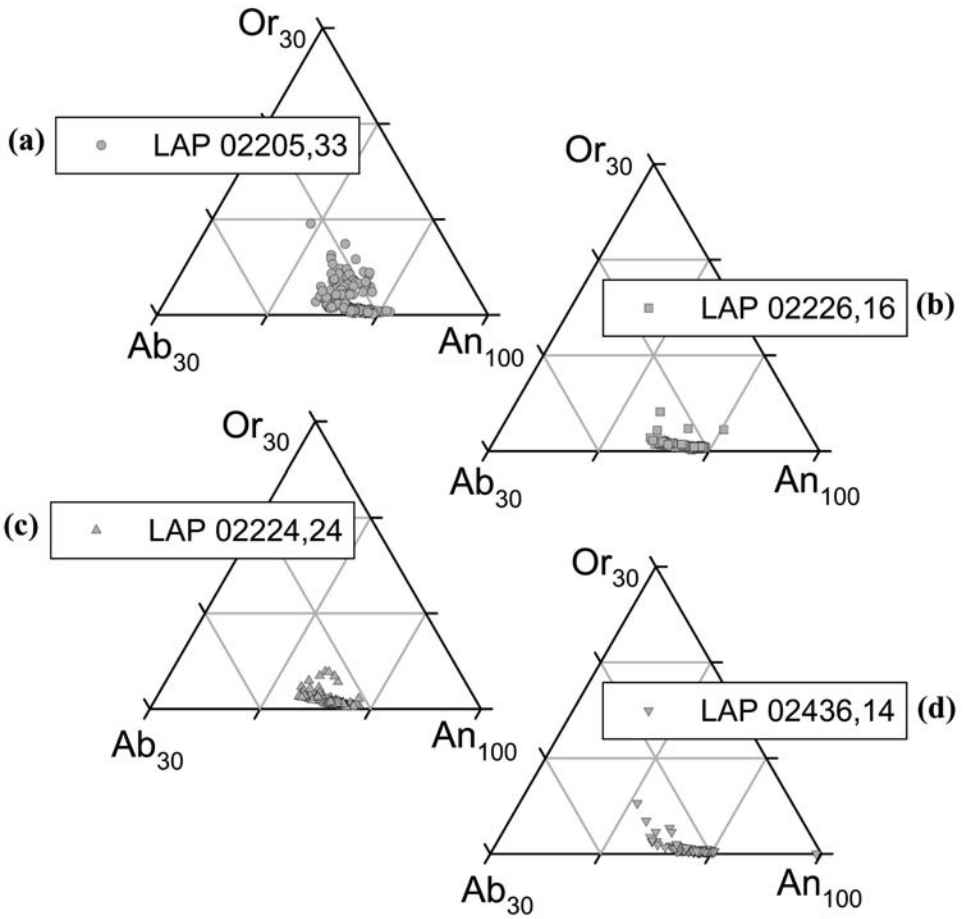

Fig. 8. Portion of feldspar ternaries showing the range of plagioclase compositions in the LAP meteorites. All show a similar range ($An_{90–80}$) and distribution, though LAP 02205,33 shows a somewhat higher proportion of evolved (high Or) compositions. This difference is an experimental artifact that resulted from taking multiple traverses on the edges of grains in that sample to elucidate zoning trends (Ab, Or enrichment; see Fig. 9). a) LAP 02205,33. b) LAP 02226,16. c) LAP 02224,24. d) LAP 02436,14.

along a common linear trend with ranges for the two meteorites that overlap (e.g., Fig 12). For nearly all elements that we measured, the most magnesian LAP subsamples (i.e., those with the most normative and presumably modal olivine) are compositionally indistinguishable from the least magnesian NWA 032 subsamples (those with the least olivine). The only elements that we determined that do not fall along a common trend for the two meteorites are Ba and K. In NWA 032, the concentrations of both of these elements are elevated as a result of terrestrial alteration in a hot desert meteorite (Fig. 13b; Fagan et al. 2002; Korotev et al. 2003b).

The difference between the average composition of LAP and NWA 032 is consistent with a loss of the earliest crystallized phases in NWA 032 relative to LAP. For major elements, removal of 4.8% olivine (average LAP core composition), 2.7% magnesian pyroxene (average LAP core composition, both high- and low-Ca), and 0.22% chromite (average LAP composition) from the average composition of NWA 032 yields a residual composition that is very similar to the average LAP composition (Table 10). For incompatible elements, the loss of ~8% of the earliest crystallized phases from NWA 032 increases the concentrations of incompatible elements in the residuum by about ~8% (assuming that olivine, pyroxene, and chromite are perfectly incompatible for all incompatible trace elements), thus accounting for about two thirds of the difference in concentrations of incompatible elements between NWA 032 and LAP (mean: NWA/LAP = 88%). Sampling error can account for the remaining ~4% difference in mean ITE concentration between LAP and the NWA 032 residuum.

The important observation, however, is that the compositional range observed among different "large" samples of lunar basalts likely derived from a single flow, e.g., samples of the Apollo 12 olivine or Apollo 12 ilmenite basalts, is equivalent to that observed among the LAP and NWA 032 subsamples in this study (Fig. 17). Furthermore, a study of 25 large samples (~10 g) taken from a vertical traverse of a single Icelandic tholeiite flow found considerable compositional variability that was not correlated

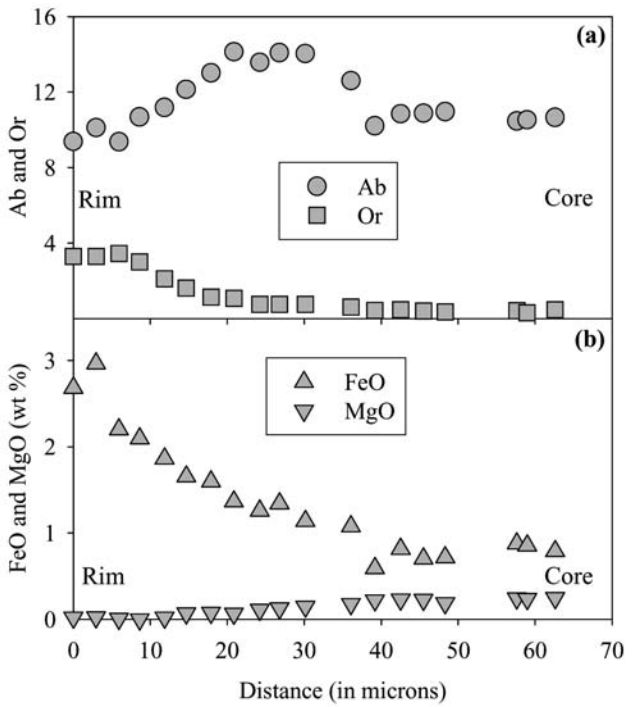

Fig. 9. Variations in Ab and Or values (a) and FeO and MgO concentrations (b) across a small, zoned plagioclase grain show that MgO steadily decreases and Or and FeO steadily increase from core to rim, but Ab first increases sharply, then gradually decreases to a value less than in the core.

with the stratigraphic location of the sample within the flow (Lindstrom and Haskin 1981). Lindstrom and Haskin (1981) attribute the compositional variability to the random distribution of the phenocrysts, groundmass minerals, and residual liquid within the flow. The range in compositions observed within the tholeiite flow (10.22–11.79 wt% FeO, 8.4–12.4 pp La) was not as quite as wide as the range in compositions among LAP and NWA 032 subsamples (21.5–23.7 wt% FeO, 10.3–15.3 pp La), but it was similar, and the average size of the tholeiite samples was more than 250 times greater than the average size of the LAP and NWA subsamples.

In summary, the geochemical and petrological similarities observed in NWA 032 and LAP indicate that these two meteorites are almost certainly source crater paired. Furthermore, given the similarities in mineral chemistry and bulk composition it appears possible that LAP and NWA 032 are from the same basalt flow on the Moon. The differences in texture are as expected if NWA 032 is from near the margin of the flow that cooled quickly after eruption, while LAP came from a more central location in the flow where it experienced a slower cooling rate. The difference in bulk chemical composition is consistent with intraflow fractionation effects and nonuniform distribution of mineral phases with respect to the small size of the analyzed samples. If cosmic ray exposure data should show that the two meteorites cannot have been

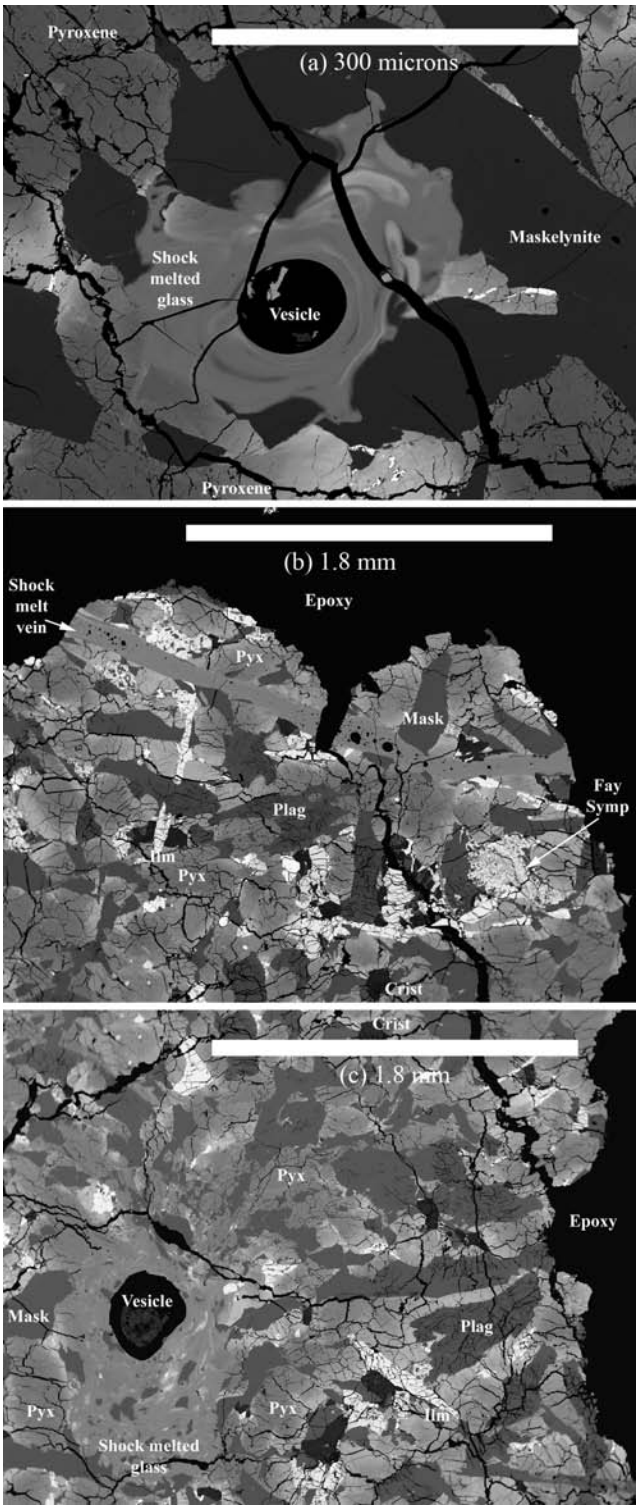

Fig. 10. a) A BSE image of a small pocket of shock-melted glass in LAP 02205,33. This glass is surrounded by maskelynite and pyroxene. Notice the schlieren (bright/dark bands) in the glass, a consequence of incomplete homogenization of the phases melted. b) A vein of shock-melted glass near the edge of LAP 02224,24 cuts across all other minerals present. c) Shock-melted glass in LAP 02224,24. Melting was incomplete so remnants of some minerals are still discernable, particularly maskelynite.

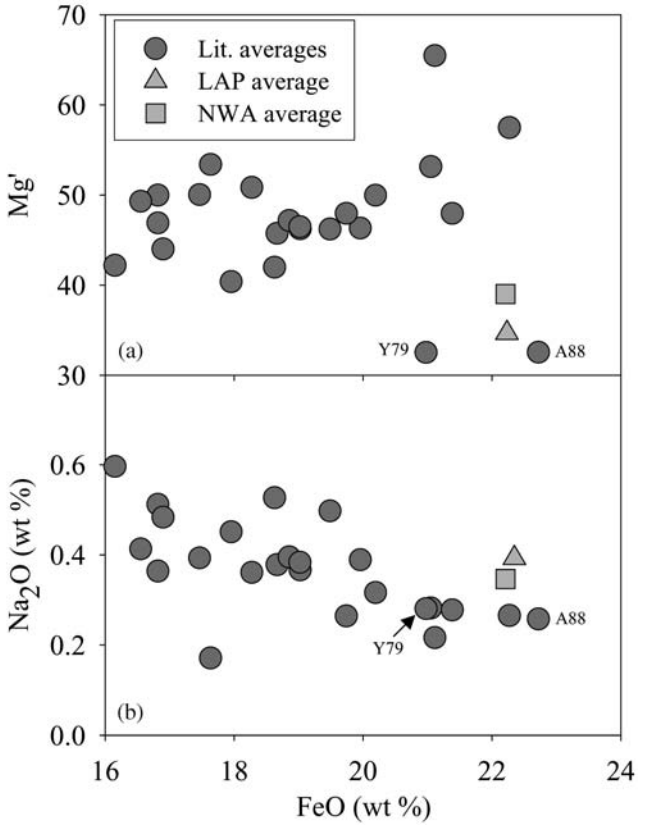

Fig. 11. FeO versus Mg′ (a) and Na_2O (b) comparing LAP (grey triangle) and NWA 032 (grey square) to the average compositions of the other basaltic lunar meteorites and Apollo and Luna basalts. The data used in these averages comes from too many references to list here (most are listed in Table 1 of Korotev 1998); the entire data set is available upon request. The LAP and NWA 032 basalts are more ferroan than all lunar basalts except lunar meteorites Asuka-881757 (A88) and Yamato-793169 (Y79). They are more alkali-rich than any of the other high-Fe lunar basalts, including A88 and Y79. In this and subsequent Figs., each circle (Lit. averages) represents the average composition of a type of Apollo or Luna basalt.

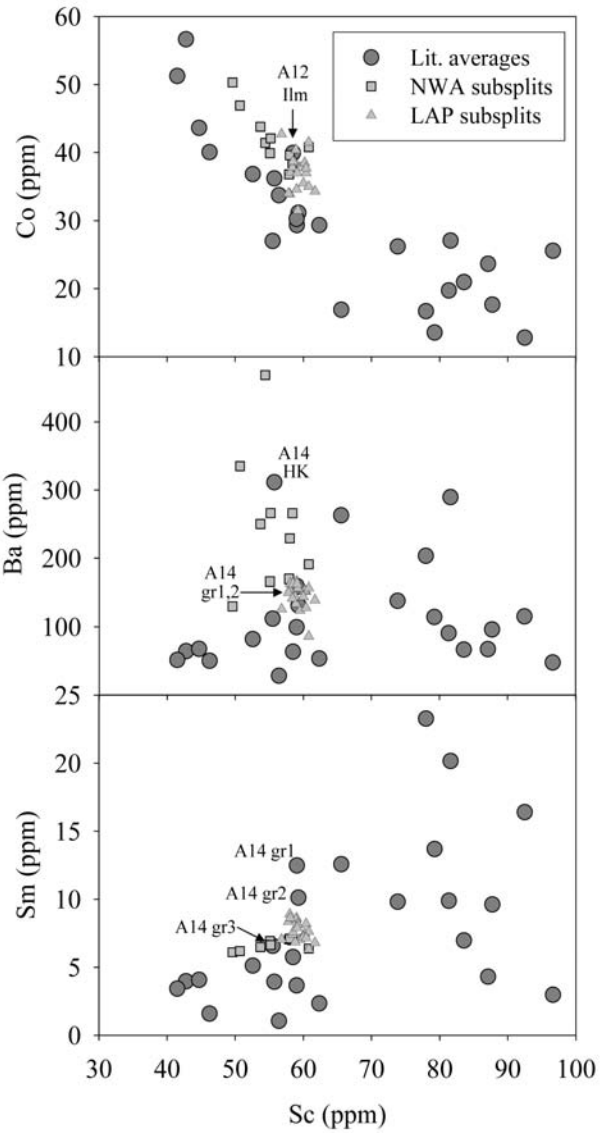

Fig. 12. Comparison of concentrations of trace elements in subsplits of LAP 02005xxx (grey triangles) and NWA 032 (grey squares) with average mare basalt compositions from the Apollo and Luna missions (dark grey circles). The data used in these averages come from too many references to list here (most are listed in Table 1 of Korotev 1998); the entire data set is available upon request. a) The subsamples of LAP 02005xxx and NWA 032 form a linear trend because of variation in modal olivine (high Co, low Sc) abundance and nearly constant clinopyroxene (low Co, high Sc) abundance. Both meteorites are enriched in Co with respect to Sc compared to other lunar basalts with comparable Sc concentrations. The exception to this is the Apollo 12 ilmenite (A12 Ilm) basalt suite. b) NWA 032 is enriched in Ba (and K) as a result of terrestrial alteration (Fagan et al. 2002). c) LAP 02005xxx and NWA 032 are enriched in incompatible elements, e.g., Sm compared to other lunar basalts with comparable Sc concentrations. As in the case of Ba, the only other basalts that are comparable or more enriched are from Apollo 14.

launched from the Moon at the same time, then the similarities discussed here are a remarkable coincidence.

Petrogenesis

Below we briefly discuss possible parent magmas and, by inference, probable source regions for LAP. Regardless of whether LAP and NWA 032 are from the same flow, their bulk chemical compositions are sufficiently similar that they should have similar parent melts and source regions. At issue is whether the parent melt and source region for LAP are similar to other lunar basalts, or whether the geochemical differences that make LAP (and NWA 032) stand apart from the rest of the lunar basalt suite require a unique parent melt and source region. Also of interest is whether or not LAP and NWA 032 can be related as fractionation products of the same parent melt. To address these issues, we used the crystallization modelling programs Magpox and Magfox by John Longhi (Longhi 1987, 1991; Longhi and Pan 1988).

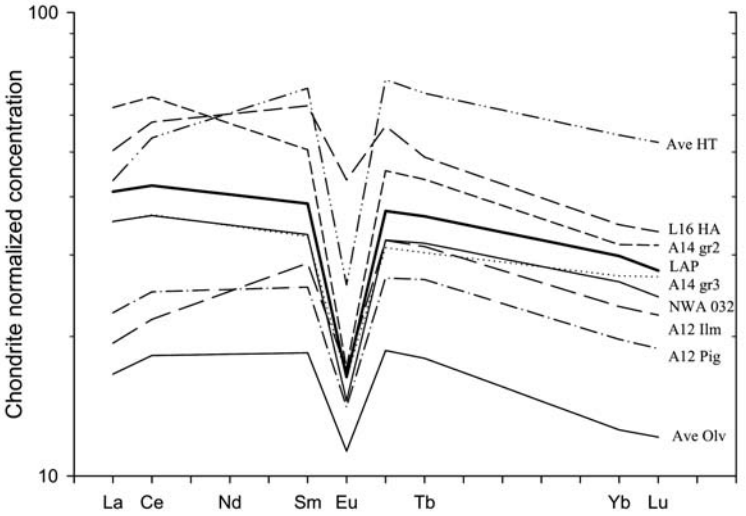

Fig. 13. Comparison of REE concentrations in LAP 02205 to those of other lunar basalts. Only the pattern for NWA 032 and the Apollo 14 group 3 high-Al basalts (A14 gr3) are similar that of LAP, although the Apollo 14 basalts have a different slope in the heavy REEs. Only those REEs listed on the axis were used in making the plot; the other values were interpolated. The high-Ti (HT) basalt pattern is an average of all Apollo 11 and Apollo 17 high-Ti basalts. The olivine basalt pattern (Ave Olv) is an average of all Apollo 12 and Apollo 15 olivine basalts. Ilm = ilmenite. Pig = pigeonite. Data used in these averages available upon request.

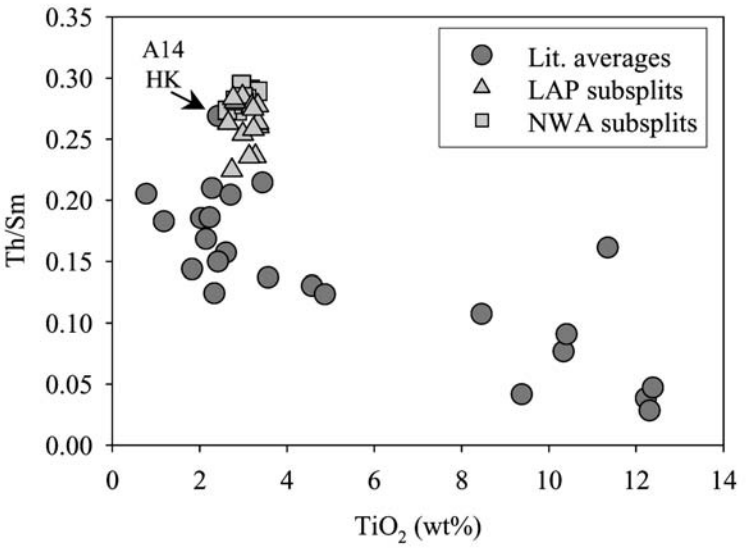

Fig. 14. NWA 032 (squares) and LAP (triangles) have greater Th/Sm ratio than any other lunar basalt (circles) except the Apollo 14 high-K basalts (HK). Data used in these averages available upon request.

These programs are based on parameterizations of liquidus boundaries and crystal-liquid partition coefficients in the model basaltic system olivine-plagioclase-pyroxene-silica.

We considered as possible parent melts the suite of lunar picritic glasses (Shearer and Papike 1993), which are thought to represent the most primitive (undifferentiated) magmas sampled on the Moon. Picritic glasses have been considered as likely parent melts of mare basalts, though no direct parent-daughter pair of picritic glass and mare basalt has so far been identified (Shearer and Papike 1993). As crystallization of a low-Ti basaltic melt tends to increase the Fe/Mg and the concentrations of TiO_2 and ITE, we infer that any plausible parent melt would have a higher Mg/Fe and lower concentrations of TiO_2 and ITEs than the bulk LAP composition. This constraint rules out the high-Ti picritic glasses.

Among the VLT and low-Ti picritic glasses, the Apollo 15 low-Ti yellow picritic glass (Table 11) is the most plausible parent melt for LAP. Starting with a melt that has the bulk composition of Apollo 15 yellow glass, the melt that remains after ~20% olivine crystallization at low pressure (0.1 kb) under equilibrium conditions is similar to the bulk

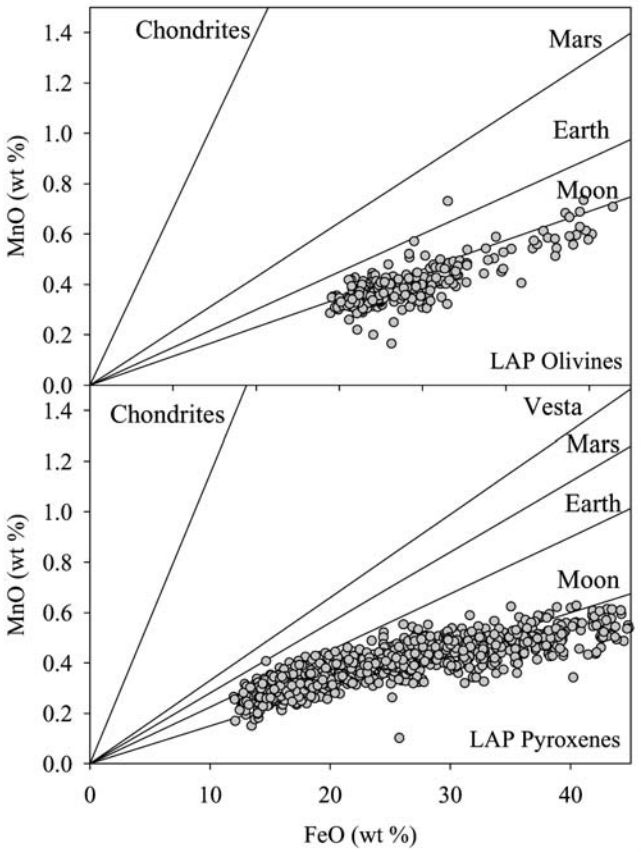

Fig. 15. FeO versus MnO concentrations in LAP olivines (top) and pyroxenes (bottom). The ratio of FeO:MnO in mafic silicates is diagnostic of the parent body on which they were formed (Dymek et al. 1976). The FeO to MnO ratio in both the LAP pyroxene and olivine is consistent with a lunar origin. The lines on both graphs are after Papike (1998).

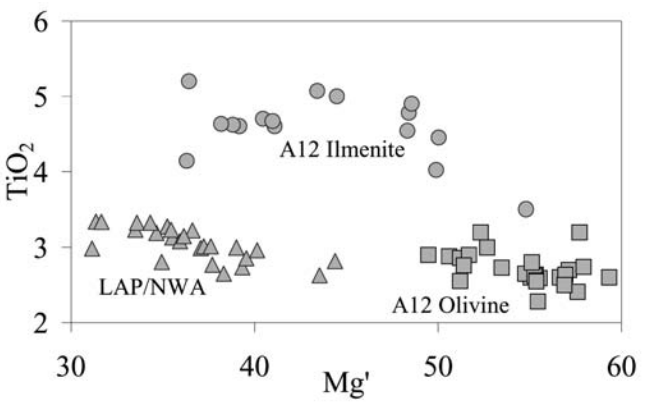

Fig. 17. The overall variability seen among all of the LAP 02005 and NWA 032 subsamples (grey triangles) is less than that observed among large samples within the Apollo 12 ilmenite basalt suite (grey circles) and only slightly greater than that among samples within the Apollo 12 olivine basalt suite (grey squares). Data used in this plot is available upon request.

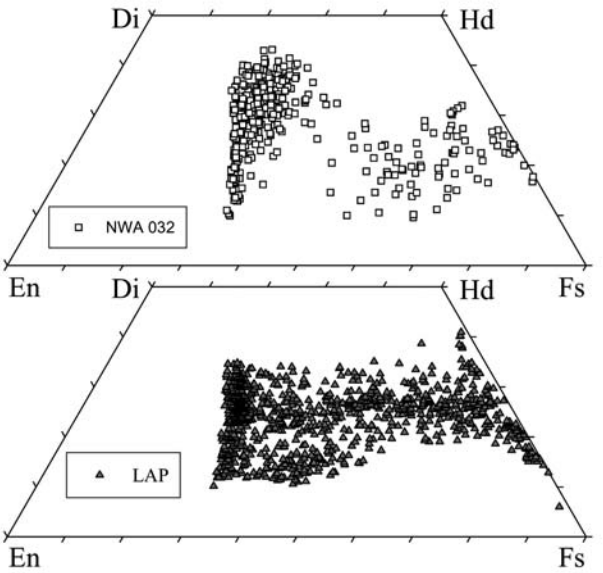

Fig. 16. Comparison of the pyroxene compositions of the four LAP stones (dark grey triangles) with the pyroxene compositions of the NWA 032 meteorite (white squares). The differences are likely a consequence of somewhat different cooling histories, LAP having cooled more slowly.

composition of LAP (Table 11). By making a few minor modifications to the bulk composition of the Apollo 15 yellow glass (change the Mg′ from 50 to 47 and the CaO/Al_2O_3 ratio from 1.03 to 1.14, both of which are within the range observed in picritic glasses), the composition of the melt that remains after ~20% olivine has crystallized is even closer to that of LAP, with only minor differences (principally in MgO concentration).

The crystallization sequence predicted at low pressure for the contemporary melt after ~20% olivine has crystallized from the modified Apollo 15 yellow glass composition does not quite match the observed crystallization sequence of LAP, which is olivine, followed closely by spinel, pigeonite, and augite, with plagioclase and ilmenite appearing later. If the residual melt crystallized at a moderate pressure (3 kb), the crystallization sequence for the resulting melt would be olivine, followed shortly by pigeonite, spinel, and augite, with plagioclase and ilmenite crystallizing later.

The similarities between the Apollo 15 yellow glass and LAP extend to their ITEs as well. Although the ITE concentrations in Apollo 15 yellow glasses show a considerable range (Shearer and Papike 1993), the concentrations of ITEs in LAP fall near the middle of this range, and the REE patterns of both yellow glass and LAP show a similar light-REE enrichment. Recent work on picritic glass beads by Hagerty et al. (2004) suggests that the Th/Sm ratio in the source areas for lunar basalts varies considerably (from 0.06 to 0.27). This means that the unusual Th/REE

Table 10. Comparing Bulk LAP and NWA 032 compositions.

	NWA ave. comp.	Core oli. ave. comp.	Core pyx. ave. comp.	Chromite ave. comp.	NWA calc.	LAP ave. comp.	% diff.
Major element concentrations							
SiO_2	44.73	36.19	50.57	0.08	45.17	45.3	–0.2
TiO_2	3.00	0.03	0.94	5.42	3.21	3.11	+3.2
Al_2O_3	9.32	0.02	2.26	11.44	10.01	9.79	+2.2
Cr_2O_3	0.40	0.25	0.80	43.87	0.31	0.31	–0.0
FeO	22.21	33.26	17.21	34.52	21.78	22.2	–2.0
MnO	0.28	0.34	0.32	0.27	0.28	0.29	–4.2
MgO	7.97	29.32	16.32	2.77	6.65	6.63	+0.2
CaO	10.57	0.36	10.94	0.04	11.12	11.09	+0.3
Na_2O	0.35	0.00	0.03	0.00	0.37	0.38	–0.8
P_2O_5	0.09	0.00	0.00	0.00	0.10	0.10	–1.5
Totals	99.00	99.79	99.40	98.41	99.00	99.21	–
% removed	–	4.8	2.7	0.22	–	–	–
Trace element concentrations							
Zr	170	–	–	–	184	183	+0.9
La	11.3	–	–	–	12.2	13.1	–6.5
Ce	29.9	–	–	–	32.4	34.7	–6.7
Nd	20	–	–	–	21	22	–4.8
Sm	6.63	–	–	–	7.19	7.74	–7.1
Eu	1.10	–	–	–	1.20	1.24	–3.8
Tb	1.57	–	–	–	1.70	1.79	–5.2
Yb	5.8	–	–	–	6.28	6.59	–4.7
Lu	0.80	–	–	–	0.87	0.92	–4.9
Hf	5.02	–	–	–	5.44	5.58	–2.7
Ta	0.63	–	–	–	0.68	0.71	–4.1
Th	1.89	–	–	–	2.05	2.04	+0.3
U	0.46	–	–	–	0.50	0.52	–3.3

The average major element compostions of LAP 02205 and NWA 032 can be related through the loss of the phases. Starting with the average NWA bulk composition and removing the equivalent of 4.8% LAP core olivine, 2.7% earliest crystallized LAP core pyroxene, and 0.2% LAP chromite, the resulting composition is very close to the bulk LAP composition. By assuming that the olivine, pyroxene, and chromite are perfectly incompatible for the listed incompatible trace elements (not true but they should be very low for most of the listed elements), we can see that the loss of ~8% of the earliest crystallized phases would account for about half of the incompatible trace element discrepancy between NWA and LAP (the average % difference is reduced from ~12% to ~4%). Some other factor, such as melt evolution, would have to be invoked in order to account for the rest of this discrepancy.

ratios seen in LAP and NWA could be inherited from their source region, and need not be a result of some type of unusual differentiation of the ascending magma (Fig. 14).

We are not advocating that Apollo 15 yellow glass is the parent melt for LAP, but rather that something similar to Apollo 15 yellow glass is a plausible parent melt composition. According to current models of the lunar mantle (e.g., Neal and Taylor 1992; Shearer and Papike 1993), the source region for a parent melt such as this would be relatively deep (>400 km) in the mantle. It would consist of both early crystallized magnesian mafic cumulates, which settled early from a lunar magma ocean, and later-crystallized Fe-Ti-ITE-rich mafic cumulates that sank into the underlying, more magnesian cumulates due to density contrast aided by partial melting due to radiogenic heating. This LAP parent melt would fractionate ~20% olivine while ascending, pond somewhere near the base of the crust (where the pressure is ~3 kb), and undergo moderate amounts of crystallization there before eruption to the surface.

NWA 032 and LAP do not appear to be sequential crystallization products of the same parent melt that has undergone varying amounts of fractionation. Only olivine is predicted to be a liquidus phase in the interval that corresponds to the difference in the bulk compositions of NWA 032 and LAP. Results shown in Table 10 have shown that simple olivine fractionation cannot account for the differences in bulk composition between NWA 032 and LAP. This supports the idea that if LAP and NWA 032 are portions of the same flow, and their compositional differences result from the random distribution of small amounts of olivine, chromite, and pyroxene in a basalt flow that eventually solidified to become LAP.

SUMMARY AND CONCLUSIONS

The four LaPaz Icefield basaltic meteorites studied here, LAP 02205, LAP 02224, LAP 02226, and LAP 02436, are low-Ti (3.1 wt%) basalts. On the basis of the oxygen isotopic

Table 11. Composition of modeled petrogenic results compared to bulk LAP composition.

	Apollo 15 yel. glass A	Modeled melt B	% diff. C	Yel glass variant D	Modeled melt E	% diff. F	LAP ave. G
SiO_2	43.8	45.3	0.0	43.8	45.7	0.8	45.3
TiO_2	2.70	3.39	9.1	2.55	3.16	1.6	3.11
Al_2O_3	8.34	10.50	7.2	8.00	9.9	1.2	9.79
Cr_2O_3	0.55	0.55	79.6	0.30	0.30	–2.2	0.31
FeO	21.8	20.7	–6.7	23.3	21.8	–1.8	22.2
MnO	0.30	0.29	0.3	0.30	0.29	0.5	0.29
MgO	12.63	7.77	17.1	11.43	6.98	5.2	6.63
CaO	8.6	10.8	–3.0	9.1	11.2	0.7	11.1
Na_2O	0.54	0.68	80.1	0.54	0.67	77	0.38
Totals	99.2	100.0	–	99.2	100.0	–	99.2
Mg'	51	40	15.3	47	36	4.6	35
CaO/Al_2O_3	1.03	1.02	–9.6	1.14	1.13	–0.4	1.13
% olv. fract.	–	19.7	–	–	19.1	–	–

Column A: Major-element composition of Apollo 15 low-Ti yellow (yel.) picritic glass as reported in Table 2, column 2b of Shearer and Papike (1993). Column D: major-element composition of a new parent melt based on the Apollo 15 yellow glass composition, but altered slightly to more closely match the requirements of LAP. Columns B and E: the modeled composition of the remaining melt after the parent melts in columns A and D (respectively) underwent equillibrium crystallization at low pressure using the Magpox program (Longhi 1987, 1991) until ~19 % olivine had crystallized (% olv. fract.). Columns C and F: a measure of how similar the modeled melt compositions in columns B and D are when compared to the average LAP bulk composition (column G). % diff. = (Modeled/LAP)/LAP*100.

signature (LAP 02205; McBride et al. 2003), FeO/MnO ratios in the mafic silicates, and a variety of other petrologic indicators, the four stones can only be of lunar origin. On the basis of overwhelming similarities in mineral assemblages and mineral compositions we conclude that the four stones are paired. Despite textural differences, mineral assemblages, mineral compositions, and bulk major- and trace-element concentrations of LAP are similar to those of NWA (Northwest Africa) 032 (Fagan et al. 2002). Among small subsamples of the two meteorites, the most magnesian subsamples of LAP 02005 are all but indistinguishable from the most ferroan subsamples of NWA 032. The textural differences between the meteorites can be attributed to different cooling histories and the minor difference in average bulk composition can largely be explained by a 7.7% loss in the earliest crystallizing phases (4.8% olivine + 2.7% pyroxene + 0.22% chromite) in LAP with respect to NWA 032. Given the similarities, we conclude that LAP and NWA 032 are almost certainly source crater paired, and that there is a possibility that they are genetically related, perhaps representing samples from different portions of a single basaltic flow. LAP is likely derived from a parent melt similar to the Apollo 15 low-Ti yellow picritic glass that has undergone moderate amounts of olivine fractionation.

Acknowledgments–We would like to thank Tim Fagan for providing the NWA 032 pyroxene probe data, Gretchen Benedix for help with the electron microprobe analyses, and Christine Floss for providing the X-ray imaging used in the modal analyses. Discussions and comments by Dr. Robert F. Dymek and Dr. Robert D. Tucker were very helpful in preparing the manuscript. Thorough and thoughtful reviews by Dr. Barbara A. Cohen, Dr. Clive R. Neal, and Dr. Kevin Righter, as well as expert editorial handling by Dr. Cyrena A. Goodrich greatly improved the finished manuscript. We would also like to thank John Schutt for the information regarding where the LAP meteorites were found in the field. This work was funded by NASA grant NAG5-10485 (L. Haskin).

Editorial Handling—Dr. Cyrena Goodrich

REFERENCES

Anand M., Taylor L. A., Neal C., Patchen A. and Kramer G. (2004) Petrology and geochemistry of LAP 02 205: A new low-Ti mare-basalt meteorite (abstract #1626). 35th Lunar and Planetary Science Conference. CD-ROM.

Arai T. and Warren P. H. 1999. Lunar meteorite Queen Alexandra Range 94281: Glass compositions and other evidence for launch pairing with Yamato-793274. *Meteoritics & Planetary Science* 34:209–243.

Bence A. E. and Papike J. J. 1972. Pyroxenes as recorders of liquid basalt petrogenesis: Chemical trends due to crystal-liquid interaction. Proceedings, 3rd Lunar Science Conference. pp. 431–469.

Collins S. J., Righter K., and Brandon A. D. 2005. Mineralogy, petrology and oxygen fugacity of the LaPaz icefield lunar basaltic meteorites and the origin of evolved lunar basalts (abstract #1141). 36th Lunar and Planetary Science Conference. CD-ROM.

Day J. M. D., Taylor L. A., Patchen A. D, Schnare D. W., and Pearson D. G. 2005. Comparative petrology and geochemistry of the LaPaz mare basalt meteorites (abstract #1419). 36th Lunar and Planetary Science Conference. CD-ROM.

Dickinson T., Taylor G. J., Keil K., Schmitt R. A., Hughes S. S., and Smith M. R. 1985. Apollo 14 aluminous mare basalts and their possible relationship to KREEP. Proceedings, 15th Lunar and Planetary Science Conference. pp. 365–374.

Donavan J. J., Hanchar J. M., Picolli P. M., Schrier M. D., Boatner L. A., Jarosewich E. 2003. A re-examination of the rare-earth-element orthophosphate standards in use for electron microprobe analysis. *The Canadian Mineralogist* 41:221–232.

Dymek R. F., Albee A. L., Chodos A. A., and Wasserburg G. J. 1976. Petrography of isotopically-dated clasts in the Kapoeta howardite and petrologic constraints on the evolution of its parent body. *Geochimica Cosmochimica Acta* 40:1115–1130.

El Goresy A., Ramdohr P., and Taylor L. A. 1971. The opaque minerals in the lunar rocks from Oceanus Procellarum. Proceedings, 2nd Lunar Science Conference. pp. 219–235.

Fagan T. J., Taylor G. J., Keil K., Bunch T. E., Wittke J. H., Korotev R. L., Jolliff B. L., Gillis J. J., Haskin L. A., Jarosewich E., Clayton R. N., Mayeda T. K., Fernandes V. A., Burgess R., Turner G., Eugster O., and Lorenzetti S. 2002. Northwest Africa 032: Product of lunar volcanism. *Meteoritics & Planetary Science* 37:371–394.

Gnos E., Hofmann B. A., Al-Kathiri A., Lorenzetti S., Eugster O., Whitehouse M. J., Villa I. M., Jull A. J. T., Eikenberg J., Spettel B., Kraehenbuehl U., Franchi I. A., Greenwood R. C. 2004. Pinpointing the source of a lunar meteorite: Implications for the evolution of the Moon. *Science* 305:657–660.

Hagerty J. J., Shearer C. K., and Vaniman D. T. Thorium and samarium in lunar pyroclastic glasses: Insights into the composition of the lunar mantle and basaltic magmatism on the Moon (abstract #1817). 35th Lunar and Planetary Science Conference. CD-ROM.

Haskin L. A., Helmke P. A., Allen R. O., Anderson M. R., Korotev R. L., and Zweifel K. A. 1971. Rare-earth elements in Apollo 12 lunar materials. Proceedings, 2nd Lunar Science Conference. pp. 1307–1317.

Haskin L. A., Jacobs J. W., Brannon J. C., and Haskin M. A. 1977. Compositional dispersions in lunar and terrestrial basalts. Proceedings, 8th Lunar Science Conference. pp. 1731–1750.

Helmke P. A. and Haskin L. A. 1972. Rare earths and other trace elements in Luna 16 soil. *Earth and Planetary Science Letters* 13:441–443.

Jarosewich E. and Boatner L. A. 1991. Rare-earth element reference samples for electron microprobe analysis. *Geostandards Newsletter* 15:397–399.

Jolliff B. L., Korotev R. L., and Haskin L. A. 1991. Geochemistry of the 2–4 mm particles from the Apollo 14 soil (14161) and implications regarding igneous components and soil forming processes. Proceedings, 21st Lunar and Planetary Science Conference. pp. 193–219.

Jolliff B. L., Rockow K. M., and Korotev R. L. 1998. Geochemistry and petrology of lunar meteorite Queen Alexandra Range 94281, a mixed mare and highland regolith breccia, with special emphasis on very-low-Ti mafic components. *Meteoritics & Planetary Science* 33:581–601.

Joy K. H., Crawford I. A., Russell S. S., and Kearsley A. 2004. Mineral chemistry of LaPaz Ice Field 02205–A new lunar basalt (abstract #1545). 35th Lunar and Planetary Science Conference. CD-ROM.

Kieffer S. W., Schaal R. B., Gibbons R. V., Hörz F., Milton D. J., and Dube A. 1976. Shocked basalt from the Lonar impact crater, India, and experimental analogs. Proceedings, 2nd Lunar Science Conference. pp. 1391–1412.

Koeberl C., Kurat G., and Brandstätter F. 1993. Gabbroic lunar mare meteorites Asuka-881757 (Asuka-31) and Yamato-793169: Geochemical and mineralogical study. *Proceedings of the NIPR Symposium on Antarctic Meteorites* 6:14–34.

Korotev R. L. 1991. Geochemical stratigraphy of two regolith cores from the central highlands of the Moon. Proceedings, 21st Lunar and Planetary Science Conference. pp. 229–289.

Korotev R. L. 1998. Concentrations of radioactive elements in lunar materials. *Journal of Geophysical Research* 103:1691–1701.

Korotev R. L., Lindstrom M. M., Lindstrom D. J., and Haskin L. A. 1983. Antarctic meteorite ALH A81005—Not just another lunar anorthositic norite. *Geophysical Research Letters* 10:829–832.

Korotev R. L., Jolliff B. L., and Rockow K. M. 1996. Lunar meteorite Queen Alexandra Range 93069 and the iron concentration of the lunar highlands surface. *Meteoritics & Planetary Science* 31: 909–924.

Korotev R. L. and Haskin L. A. 1975. Inhomogeneity of trace element distributions from studies of the rare earths and other elements in size fractions of crushed lunar basalt 70135. Conference on Origins of Mare Basalts and Their Implications for Lunar Evolution. LPI Contribution #234. Houston, Texas: Lunar and Planetary Science Institute. pp. 86–90.

Korotev R. L., Jolliff B. L., Zeigler R. A., and Haskin L. A. 2003a. Compositional constraints on the launch pairing of three brecciated lunar meteorites of basaltic composition. *Antarctic Meteorite Research* 16:152–175.

Korotev R. L., Jolliff B. L., Zeigler R. A., Gillis J. J., and Haskin L. A. 2003b. Feldspathic lunar meteorites and their implications for compositional remote sensing of the lunar surface and the composition of the lunar crust. *Geochimica Cosmochimica Acta* 67:4895–4923.

Lindstrom M. M. and Haskin L. A. 1978. Causes of compositional variations within mare basalt suites. Proceedings, 10th Lunar and Planetary Science Conference. pp. 465–486.

Lindstrom M. M. and Haskin L. A. 1981. Compositional inhomogeneities in a single Icelandic tholeiite flow. *Geochimica et Cosmochimica Acta* 45:15–31.

Lindstrom D. J. and Korotev R. L. 1982. TEABAGS: Computer programs for instrumental neutron activation analysis. *Journal of Radioanalytical Chemistry* 70:439–458.

Longhi J. 1987. On the connection between mare basalts and picritic glasses. Proceedings, 17th Lunar and Planetary Science Conference. pp. 349–360.

Longhi J. 1991. Comparative liquidus equilibria of hypersthene-normative basalts at low pressure. *American Mineralogist* 76: 785–800.

Longhi J. and Pan V. 1988. A reconnaissance study of phase boundaries in low-alkali basaltic liquids. *Journal of Petrology* 29:115–147.

Ma M.-S., Schmitt R. A., Nielsen R. L., Taylor G. J., Warner R. D., and Keil K. 1979. Petrogenesis of Luna 16 aluminous mare basalts. *Geophysical Research Letters* 6:909–912.

McBride K., McCoy T., and Welzenbach L. 2003. LAP 02205. *Antarctic Meteorite Newsletter* 27(1).

McBride K., McCoy T., and Welzenbach L. 2004a. LAP 02224, 02226, and 02436. *Antarctic Meteorite Newsletter* 26(2).

McBride K., McCoy T., and Welzenbach L. 2004b. LAP 03632. *Antarctic Meteorite Newsletter* 27(3).

Neal C. R. and Taylor L. A. 1992. Petrogenesis of mare basalts: A record of lunar volcanism. *Geochimica Cosmochimica Acta* 56: 2177–2211.

Neal C. R., Taylor L. A., and Patchen A. D. 1989a. High alumina (HA) and very high potassium (VHK) basalt clasts from Apollo 14 breccias, Part 1—Mineralogy and petrology: Evidence of crystallization from evolving magmas. Proceedings, 19th Lunar and Planetary Science Conference. pp. 137–145.

Neal C. R., Taylor L. A., Schmitt R. A., Hughes S. S., and Lindstrom M. M., 1989b. High alumina (HA) and very high potassium (VHK) basalt clasts from Apollo 14 breccias, Part 1—Whole rock geochemistry: Further evidence for combined assimilation

and fractional crystallization within the lunar crust. Proceedings, 19th Lunar and Planetary Science Conference. pp. 147–161.

Neal C. R., Hacker M. D., Snyder G. A., Taylor L. A., Liu Y.-G., and Schmitt R. A., 1994. Basalt generation at the Apollo 12 site, Part I: New data, classification, and re-evaluation. *Meteoritics* 29: 334–348.

Ostertag R. 1983. Shock experiments on feldspar crystals. Proceedings, 14th Lunar and Planetary Science Conference. pp. 364–376.

Papike J. J. 1998. Comparative planetary mineralogy: Chemistry of melt-derived pyroxene, feldspar, and olivine. In *Planetary materials*, edited by Papike J. J. Washington, D.C.: Mineralogical Society of America. pp 7-1–7-11.

Philpotts J. A., Schnetzler C. C., Bottino M. L., Schuhmann S., and Thomas H. H. 1972. Luna 16: Some Li, K, Rb, Sr, Ba, rare-earth, Zr, and Hf concentrations. *Earth and Planetary Science Letters* 13:429–435.

Rhodes J. M., Blanchard D. P., Dungan M. A., Brannon J. C., and Rodgers K. V. 1977. Chemistry of Apollo 12 mare basalts: Magma types and fractionation processes. Proceedings, 8th Lunar Science Conference. pp. 1305–1338.

Ryder G., and Ostertag R. 1983. ALHA 81005; Moon, Mars, petrography, and Giordano Bruno. *Geophysical Research Letters* 10:791–794.

Ryder G. and Schuraytz B. C. 2001. Chemical variation of the large Apollo 15 olivine-normative mare basalt rock samples. *Journal of Geophysical Research* 106:1435–1451.

Schaal R. B., Hörz F., Thompson T. D., and Bauer J. F. 1979. Shock metamorphism of granulated lunar basalt. Proceedings, 10th Lunar and Planetary Science Conference. pp. 2547–2571.

Schmincke, H.-U. 1967. Stratigraphy and petrography of four upper Yakima basalt flows in south-central Washington. *Geological Society of America Bulletin* 78:1385–1422.

Shearer C. K. and Papike J. J. 1993. Basaltic magmatism on the Moon: A perspective from volcanic picritic glass beads. *Geochimica Cosmochimica Acta* 57:4785–4812.

Shervais J. W., Taylor L. A., and Lindstrom M. M. 1985. Apollo 14 mare basalts: Petrology and geochemistry of clasts from consortium breccia 14321. Proceedings, 15th Lunar and Planetary Science Conference. pp. 375–395.

Stöffler D. and Hornemann U. 1972. Quartz and Feldspar glasses produced by natural and experimental shock. *Meteoritics* 7:371–394.

Thalmann C., Eugster O., Herzog G. F., Klein J., Krähenbühl U., Vogt S., and Xue S. 1996. History of lunar meteorites Queen Alexandra Range 93069, Asuka-881757, and Yamato-793169 based on noble gas isotopic abundances, radionuclide concentrations, and chemical composition. *Meteoritics & Planetary Science* 31:857–868.

Thompson J. B., Jr. 1982. Compositional space: An algebraic and geometric approach. In *Characterization of metamorphism through mineral equilibria,* edited by Ferry J. M. Washington, D.C.: Mineralogical Society of America. pp. 1–31.

Warren P. H. 1994. Lunar and Martian meteorite delivery systems. *Icarus* 111:338–363.

Warren P. H. and Kallemeyn G. W. 1993. Geochemical investigations of two lunar mare meteorites: Yamato-793169 and Asuka-881757. *Proceedings of the NIPR Symposium on Antarctic Meteorites* 6:35–57.